2020-01-01

Design And Characterization Of Thermal Inkjet Bioprinted Constructs For The Treatment Of Diabetic Foot Ulcers And Other Wound Healing Impaired Conditions

Luis Horacio Solis
University of Texas at El Paso

DESIGN AND CHARACTERIZATION OF THERMAL INKJET BIOPRINTED CONSTRUCTS FOR THE TREATMENT OF DIABETIC FOOT ULCERS AND OTHER WOUND HEALING IMPAIRED CONDITIONS

LUIS HORACIO SOLIS

Doctoral Program in Biomedical Engineering

APPROVED:

Thomas Boland, Ph.D., Chair

Renato Aguilera, Ph.D.

Tamis Bright, M.D.

Robert Kirken, Ph.D.

Stephen L. Crites, Jr., Ph.D.
Dean of the Graduate School

Dedication

To my beautiful family:

My wife, Cynthia, mi chango, Ivette, y a mi pollito, Luis Horacio II

To my parents:

Ramiro Horacio and Carlota Amalia

To my brothers:

Ramiro CeAcatl and Carlos German

To my committee members:

Dr. Thomas Boland, Dr. Renato Aguilera, Dr. Tamis Bright, and Dr. Robert Kirken

DESIGN AND CHARACTERIZATION OF THERMAL INKJET BIOPRINTED CONSTRUCTS FOR THE TREATMENT OF DIABETIC FOOT ULCERS AND OTHER WOUND HEALING IMPAIRED CONDITIONS

by

LUIS HORACIO SOLIS, MPH

DISSERTATION

Presented to the Faculty of the Graduate School of

The University of Texas at El Paso

in Partial Fulfillment

of the Requirements

for the Degree of

DOCTOR OF PHILOSOPHY

Biomedical Engineering

THE UNIVERSITY OF TEXAS AT EL PASO

May 2020

Acknowledgements

I would like to thank Dr. Thomas Boland for allowing me to be part of his research group. I thank him for his guidance and assistance, as well as for the lab space, equipment, and supplies that he furnished in order to complete this work. I would also like to acknowledge my committee members, Dr. Renato Aguilera, Dr. Tamis Bright, and Dr. Robert Kirken for providing me with their open accessibility and valuable time to discuss molecular biology concepts and experimental setup designs during my Ph.D. education.

I thank all my friends for all the many hours working inside and outside of the lab, Julio Rincon, Carlos Serna III, Michael Furth, Aleli Mojica-Campbell, Yoshira Ayala, Emmanuel Utreras, Alfredo Ornelas, Mario Cano (whose office and home were also a blessing in my final hours of writing), Luis Barrera, and Andrew Pardo. My sincerest appreciation to our collaborators, Denisse Gutierrez, and Dr. Armando Varela-Ramirez, whom I consider my mentor and a huge strength of the BBRC. Yoshira Ayala, and Susana Portillo, without whom these results would not have been realized. I would like to make a special acknowledgement to Beu Oropeza, Daisy Alvarado, Valeria Altamirano, Jesus Cedeno, Dante Chaparro Vega, Octavio Cordova, Isaac Deaguero, Erwin Delgado, Jesus Castor, Mirsa Gonzalez-Favela, Michael Furth, Mario Garcia, Alba Leyva, Emilio Loera, Gisela Lopez, Fernanda Lugo, Tania Miramontes, Erik Munoz, Paola Rodriguez, Carlos Serna III, Leila Subia, and Arahim Zuniga-Herrera for their contribution in our *in vivo* data as a result of the BME histology course.

My deepest gratitude to Dr. Aguilera for providing and allowing me to be part of the RISE program under the Department of Biological Sciences. Additionally, I am exceptionally grateful to Dr. Isela Ocegueda, Dr. Aaron Waggoner, and Dr. Shannon Connelly from the UTEP Graduate

School for awarding me two Dodson Research Grants plus the Dissertation Completion Fellowship Award which again without all of this funding this work would not have been possible.

I would like to give a special acknowledgement to my wife and kids. Thank you Panchita for giving me two incredible kids and for all your understanding and unwavering support throughout my educational responsibilities. Thank you Chango for all your love and for showing me how beautiful it is to be a dad. Thank you Pollito for being an amazing blessing and addition to our wonderful family. We were dying to meet you and now that you are here, we can't wait to hear you laugh and talk.

Abstract

Tissue engineering (TE) is a multidisciplinary practice focused on developing patient-specific constructs to repair, regenerate, or replace injured tissues and organs. One biofabrication process that has gained tremendous momentum in this field is bioprinting. Most, if not all bioprinting modalities embody the same principles of heat and shear due to mechanical forces or friction as cells are forced through narrow orifices. While it is important to examine the interaction between host and implanted constructs, it is also crucial to understand the direct effects that these bioprinting technologies have on cells before embedding them into TE applications.

The purpose of this work is to determine the effects of thermal inkjet bioprinting (TIB) on cellular angiogenesis *in vitro*. Our *in vivo* histological analysis of implanted constructs containing TIB endothelial cells (ECs) in B-17SCID mice demonstrated significantly higher number of capillary-like structures as compared to constructs with manually pipetted (MP) ECs. Additionally, *in vitro* cellular morphological differences between TIB- and MP-ECs were noted. TIB cells had elongated protrusions at 5–6 times the size of MP cells. Moreover, an Annexin V-FITC and PI apoptosis assay showed a 75% apoptosis among TIB cells as compared to MP cells via flow cytometry analysis. After a 3-day incubation period, however, TIB cells demonstrated significantly higher viability as compared to the control group. Also, cytokine expression was assessed with the use of Milliplex magnetic bead panels, which confirmed significant overexpression of HSP70, IL-1α, VEGF-A, IL-8, and FGF-1 among TIB cells as compared to the control. Furthermore, a Human phospho-kinase array to determine intracellular kinase and protein activation showed a significant over activation of HSP27 and HSP60 in TIB cells as compared to MP cells as well as a decreased proliferative state among TIB-ECs.

In all, we have demonstrated that constructs containing TIB-ECs offers an alternative method to inducing microvascular networks *in vivo*. Our *in vitro* data also supports our findings as they translate *in vivo*. The ability to create vast capillary networks, coupled with the fixed printing parameters of our TIB technology (i.e. heat, pressure, nozzle size, droplet size, and velocity) allows for versatile and repeatable means to create these constructs. Future *in vitro* work with appropriate controls for mechanical stress or possibly printing with the cartridge submerged within media to control for cellular stretching are recommended. Also, *in vivo* work with impaired wound healing such as a diabetic foot ulcer model are also suggested. Finally, a comparative study among different TIB modalities are also recommended. Looking ahead, bioengineered constructs using our TIB technology may find potential applications in organ on a chip, drug testing, and autonomic healing applications.

Table of Contents

List of Tables

List of Figures

Chapter 1: Introduction

Tissue engineering (TE) is a multidisciplinary practice focused on developing patient-specific constructs to repair, regenerate, or replace injured tissues and organs. Using a combination of biomaterials, cells, growth factors, and engineering technologies, artificial tissues can be created to regenerate or repair their injured counterparts. One biofabrication process that has gained tremendous momentum in this field is bioprinting. Little is known, however, about the direct effects that the bioprinting process inflicts on cells. Most, if not all bioprinting modalities embody the same principles of heat and shear due to mechanical forces or friction as cells are forced through narrow orifices. While it is important to examine the interaction between host and implanted bioengineered constructs, it is also crucial to understand the direct effects that these bioprinting technologies have on cells before embedding them into TE applications. Understanding these direct effects could facilitate in improving construct designs or to optimize the desired outcomes. The purpose of this work is to determine the effects of thermal inkjet bioprinting (TIB) on cellular angiogenesis *in vitro*.

Dissertation Overview

In Chapter 2, a literature review is provided focusing on diabetic foot ulcers (DFUs), the wound healing process, as well as the current treatments for DFUs. In Chapter 3, a brief history of the TIB technology along with its mechanism are described. Moreover, the induction of *in vivo* microvascular networks among implanted constructs with TIB-EC are reported. In Chapter 4, *in vitro* characterization of TIB-ECs is defined, including cell morphology, cell viability, cytokine expression, and kinase phosphorylation. Finally, the key conclusions of my Ph.D. work along with the limitations and future work recommendations are summarized in Chapter 5.

Chapter 2: Literature Review

2.1 Diabetic Foot Ulcers

Diabetic foot ulcers (DFUs) remain a serious complication of diabetes resulting in significant morbidity, mortality, and healthcare expenses among patients. There were 285 million people affected by diabetes in 2010 and more than 366 million are projected to have this disease by 2030 [1][2]. DFUs affect 15-34% of all diabetic patients within their lifetime [1][2][3][4], resulting in 84% of all lower-leg amputations worldwide [2][3][5][6][7][8]. This translates into a leg being amputated every 30 seconds around the world [1]. Most alarming is the 44% mortality rate within the first year after an amputation [9], which becomes 30-50% within 3 years [10], and 77% within 5 years [9][7]. In addition to the high burden of medical expenses [1]. The cost for the management of DFUs in the U.S. is between $9-13 billion annually [8]. Current treatment modalities consist of offloading devices and artificial skin substitutes.

2.2 Wound Management Practices for DFUs

2.2.1 Offloading Devices

Total contact casts (TCCs) and removable cast walkers (RCWs) are the most commonly used offloading devices used for the treatment of DFUs. TCCs are universally recognized as the gold standard devices for the treatment of DFUs [11][12][13][14][15][16][8]; however, patient usage compliance is relatively low. Armstrong et al. [11] monitored DFU patients being treated with a RCW device for seven days and found a 28% compliance rate. Reasons for poor compliance among patients include, impaired daily activities such as sleeping or showering and worsening postural instability [12]. Crews et al. [16] found that postural instability was strongly associated with poor offloading treatment compliance due to the device being bulky and heavy and having forced fixation, resulting in changes with the patient's normal gait. They note that even among healthy individuals, gait, balance, and reaching functionality are all affected when an offloading boot is worn. Thus, in comparison to diabetic patients who suffer from neuropathy-related changes,

the challenges observed among healthy individuals might be more pronounced in DFU patients who wear these offloading devices [16]. Not only is compliance low among patients, but clinicians are not implementing their use, which is concerning. Among 901 clinics in 48 states and D.C., only 1.7% used TCCs for the treatment of DFUs; 15.2% used RWCs; 2.6% used other devices such as therapeutic shoes; and 12.3% used complete non-weight-bearing (NWB) devices such as crutches and wheelchairs. Interestingly, 58.1% did not consider TCCs as the golf standard of treatment for DFUs and 45.5% did not use TCCs as an offloading device [12]. The authors conclude that in reality, clinicians understand that reducing pressure, shear, and repetitive injury do dramatically affect the outcomes of DFU treatments; however, when it comes to TCCs, their application requires skill, they are labor intensive, and the procedure is time consuming [8] and clinics may not have the necessary manpower available [12]. Also, the low percentage use of RCWs might be related to issues of cost and lack of reimbursement in the U.S. For these reasons clinicians tend to use other offloading methods for the treatment of DFUs [12] and/or make use of advanced wound care technologies such as artificial skin substitutes.

2.2.2 Tissue Engineered Skin Substitutes

Artificial skin substitutes were developed to assist in the treatment of superficial wounds. These skin substitutes are divided into two groups: allogenic cell-containing constructs, such as Apligraf and Dermagraft, and acellular matrices like Oasis and MatriStem [17]. In a systematic review for the treatment of DFUs with skin substitutes, researchers concluded that compared to treatment alone, additional treatment with skin substitutes, could reduce the healing time of DFUs and decrease the need for amputations [18]. However, skin substitutes are relatively expensive, especially since treatment of a DFU lasts several months and numerous skin substitute applications are needed ($5,000 for cell-containing constructs vs $2,000 for acellular matrices for the same length of time to heal a DFU). Interestingly, the authors found no conclusive evidence for the effectiveness between the two types of skin substitutes in the treatment of DFUs [17].

While these skin substitutes provide the adequate wound healing parameters (e.g. low pH, moisture, antimicrobial ingredients, etc.), they do not provide the angiogenic properties required for proper wound healing. Key proangiogenic factors include fibroblast growth factor 2 (FGF-2), interleukin 8 (IL-8), platelet-derived growth factor (PDGF), placental growth factor (PlGF), transforming growth factor-β, and vascular endothelial growth factor (VEGF) [19].

2.3 Wound Healing

The wound healing process occurs in four major steps: a) hemostatic, b) inflammatory, c) proliferative, and d) remodeling [20]. Granulation tissue, which forms during the proliferative stage, is the hallmark of a positive wound healing response. It is during this step that fibrovascular tissue containing fibroblasts, capillaries, and collagen is formed [21]. Not only is angiogenesis critical for the formation of granulation tissue [20][21][22][23], but it is also necessary to transfer of nutrients and oxygen in addition to removing waste metabolites from the wounded area as it promotes the regeneration of new tissue [21][22].

2.4 Tissue Engineering Challenge: Angiogenesis

Current tissue engineering strategies for the induction of angiogenesis include scaffold design such as sacrificial constructs, material functionalization, microfabrication, and bioreactors. Additionally, genetic manipulation strategies through stem cells, miRNA induction, and synthetic polymers have demonstrate great strides in vascularization efforts [24]. Despite all this progress, the challenges of architecture, biological control, bioavailability, biodegradability, host immune responses, stem cell fate, and the understanding of biomolecular signaling pathways of angiogenic induction remain. Comprehensive reviews on all these different approaches have been recently published [25][26][27][24].

Chapter 3: Thermal Inkjet Bioprinting (TIB): A Promising Approach to Angiogenic Induction

3.1 TIB Technology

Bioprinting is the process of depositing cells with the help of a modified printer. More specifically, thermal inkjet bioprinting (TIB) technology has the ability to deliver cells, growth factors, and biomaterial scaffolds to create various shapes and thickness with digital control [6]. The thermal inkjet printer is one of the oldest printing technologies using drop-on-demand (DOD) technology patented in 1951 [28]. In 2003, Cris Wilson and Thomas Boland were the first pioneers to modify an HP 660C desktop thermal inkjet printer for the purposes of printing proteins and cells for drug screening and tissue engineering applications [29]. Furthermore, Boland et al., 2003, demonstrated that 3D layer by layer constructs could be developed using a thermosensitive gel with the use of TIB technology [30].

The printing process of TIB can be conceptualized in three steps as depicted in Figure 1: 1) the heating of thermal actuator or resistor inside the chamber of a modified ink cartridge heats up to approximately 300 °C for 2 microseconds [6]; 2) a bioink bubble forms on the surface of the resistor which will eventually produce enough pressure to overcome the surface tension; and 3) bioink droplets are ejected out of the cartridge nozzles as bubbles collapse inside the chamber [28]. This process repeats throughout the bioprinting process in pulses of 10 μs. Modeling experiments demonstrate that the initial 300 °C heat of the resistor actually disperses into the bioink and its kinetic energy resulting in an actual temperature between 4 and 10 degrees above the ambient temperature thus useful for bioprinting applications [6][31].

Figure 2 illustrates this process further, demonstrating a compilation of high-speed photographic images of ejected droplets from an DOD inkjet printer. Briefly, when the ink droplet first exits the nozzle, it forms a jet (Figure 2A). Secondly, while the droplet is still attached to the nozzle, it deforms as a stretched-out tail or ligament, characteristic of inkjet droplets, Figure 2B.

Finally, while part of the drop returns to the nozzle, the complete tail joins the ejected drop and may break up into small satellite drops, Figure 2C [32].

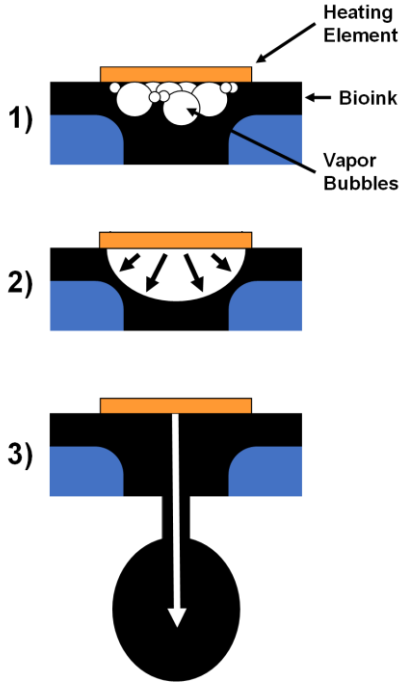

Figure 1. Mechanism behind the TIB technology.

1) Vapor bubbles develop on the heating element. 2) Formation of a larger vapor bubble. 3) The vapor bubble collapses and a single drop of ink is ejected.

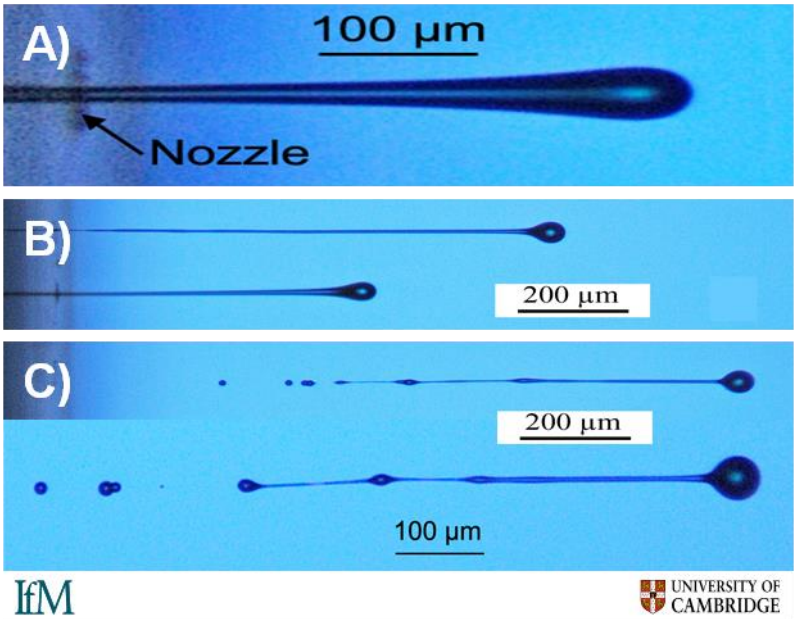

Figure 2. High speed photographs showing droplets ejected from drop-on-demand inkjet nozzles (Reproduced and rearranged from the original images to demonstrate the sequence of events while retaining the original content from a PowerPoint attachment from Dr. Ian Hutchings, Institute of Manufacturing at The University of Cambridge via email correspondence).

A) Jet of ink stretching out from an inkjet nozzle. **B)** Elongated tail of droplet connected to the inkjet nozzle. **C)** Midair inkjet droplets demonstrating the elongated tails attached to the droplets and formation of smaller satellite drops.

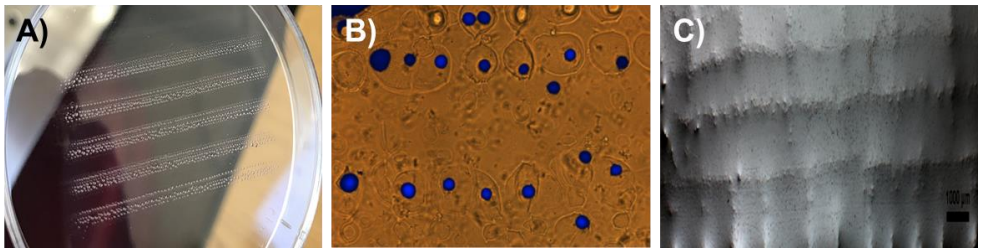

Figure 3. Demonstration of TIB droplets.

A) TIB droplets on a Petri dish. **B)** TIB-ECs on an alginate construct. ECs appear in blue due to DAPI staining. Notice that almost every bioink droplet contained a single cell as well as the impressions from smaller satellite droplets. **C)** Topology of a TIB alginate construct demonstrating droplet impressions.

For the purposes of this entire project, a more complete description of the thermal inkjet printer developed in our laboratory can be found in De Maria, C., et al. 2010 [33]. Table 1 depicts the typical range parameters for thermal inkjet printers.

Table 1. Thermal inkjet printer parameters.

Parameters	Typical Range
Cartridge size	HP 20, 26
Number of nozzles on cartridge	54
Nozzle size of cartridge	40-100 μm
Operating frequency	3-25 kHz
Printed droplet volume	50-500 pL
Heating temperature	300 °C
Pulse rate	2-10 μs
Refractory rate	200 μs
Temperature of bioink	46 °C
Printing droplet velocity	3-15 m s-1

3.2 *In Vitro* Microvasculature Fabrication using TIB Technology

According to Cui, X. and Boland, T. (2009), a three-dimensional channel lined with human microvascular endothelial cells (HMVECs) was made possible with the use of TIB technology. In their study, they describe the creation of a tubular structure with the use of fibrin construct laden with TIB-ECs. Their microvascular structure demonstrated EC integrity at 14 days, but a much richer confluency at day 21 [34][6]. These findings demonstrate that TIB technology could be used for the fabrication of microvasculature structures in tissue engineering or regenerative medicine applications.

3.3 TIB Technology Induces Angiogenesis

Our lab has been developing TIB cell laden collage-fibrin and alginate-gelatin hydrogel constructs for over a decade and have grafted and implanted these constructs in/on mice for *in vivo* studies. We hypothesize that constructs containing TIB-ECs induce microvascular networks *in vivo* due to the heat and mechanical forces of the TIB process. Yanez, M. et al., (2015), developed a TIB artificial bi-layered skin graft comprised of collagen, fibrin, HMVECs, fibroblasts, and keratinocytes. Interestingly, not only did her bi-layered skin graft accelerate wound healing much faster (wound contraction was significantly lower after 4 and 6 weeks, $p < 0.05$) than a commercial

dressing, but she discovered HMVEC capillary-like networks in the TIB-graft mouse model [35]. The investigators note that it was unknown if the HMVECs anastomosed with the vascularity of the mouse model or if the human endothelial cells were recruited as the wound was healing, however, it is compelling that TIB technology possibly induced the induction of angiogenesis *in vivo*.

Additionally, TIB-HMVECs in alginate-gelatin constructs were subcutaneously implanted in SCID mice for 4 weeks. As a result, TIB-HMVECs had a nine-fold increase of capillary-like structures as compared to the control groups (manuscript in progress). One year later, the same TIB-HMVEC alginate/gelatin constructs protocol was carried out and implanted in a humanized mouse model. Again, similar findings were demonstrated among TIB-HMVEC constructs as compared to control groups (data collection in progress).

3.4 Materials and Methods

Cell Culture

Pancreatic mouse beta cells, βTC-6 (ATCC® CRL-11506TM), were cultured in DMEM (Cellgro) supplemented with 1% pen/strep (HyClone) and 15% FBS (Seradigm). Human Microvascular Endothelial Cells (HMVECs) (Lonza) were grown in EBM-2 supplemented with the EGM-2 Bullet Kit (Lonza). Both cell types were subcultured and maintained at 37 ˚C in a 5% CO_2 environment.

Preparation of alginate mixtures and cell-containing hydrogels

Alginic acid powder (Acros Organics) and gelatin type B (Fisher Scientific) were both dissolved at 2% and 5% w/v in respective concentrations in PBS and sterilized via autoclave. Five alginate/gelatin constructs or scaffolds were prepared as follows: 1) Bioprinted HMVECs; 2)

Bioprinted HMVECs and βTC-6 cells; 3) Manually pipetted HMVECs; 4) Manually pipetted HMVECs and βTC-6 cells; and 5) Scaffold without any cells served as a negative control.

TIB constructs

HMVECs were trypsinized, counted, and mixed in a bioink solution of 0.15 M $CaCl_2$ in milli-Q water at a concentration of $2x10^6$ cells/ml. Four hundred microliters of pre-crosslinked alginate/gelatin solution were spread out evenly on a microscope slide using the side of the pipette tip and placed on the deposition plate the thermal inkjet printer. Two hundred microliters of bioink were loaded inside a modified printer cartridge and bioprinted in a layer-by-layer approach. The same process was repeated for βTC-6 cells and for the combination of the two cell types. After printing, the slide was dipped in a 100 x 15 mm petri dish containing 0.15 M $CaCl_2$ and allowed to crosslink for 10 minutes at room temperature. Once crosslinked the hydrogels were cut into 1 x 1 cm pieces with a scalpel and placed in a 60 x 15 mm petri dish with corresponding complete media. Co-culture media consisted of 50%/50% corresponding media. Complete constructs were maintained at 37 °C in a 5% CO_2 environment 1 hour before implantation.

Manually pipetted constructs

$2x10^6$ HMVECs were mixed in 400µl of the pre-crosslinked alginate/gelation solution and spread out evenly on a microscope slide as stated before. The same process was repeated as stated above for βTC-6 cells, combined cells, crossliking, cutting, and maintenance prior to implantation.

Surgical implantations of constructs

All bioengineered constructs were subcutaneously implanted in the dorsal cranial cervical area of 24 female B-17SCID mice following an approved animal protocol by the Institutional Animal Care and Use Committee (IACUC) at UTEP. The B-17SCID mice were purchased from the Jackson Laboratory and housed in The Border Biomedical Research Center (BBRC) at UTEP.

NOTE: The surgical implantation procedure, tissue excision, and histological analysis were performed by graduate and undergraduate students as part of a BME course taught by Beu Oropeza, a lab member in our laboratory. Students were divided into groups of 3-4 and were given 3 mice per group. Table 2 lists the eight different groups and the describes the types of constructs that were implanted by treatment group.

Briefly, on the day of the surgery, the mice were given an initial subcutaneous injection using buprenorphine (0.05-1.0 mg/kg) and maintained with vaporized isoflurane (4-5%) in an induction chamber. The animals were then placed on a warmed heating platform while maintaining the administration of isoflurane (1-3%) in oxygen via a nose cone and a precision vaporizer. A 1-1.5 cm full thickness skin incision penetrating down to the subcutaneous tissue was created on the dorsal cranial cervical area of each mice. The implant was placed in the pocket of the prepared site and closed with a 5-0 monofilament nylon suture using a simple interrupted pattern. Mice were continuously monitored until the return the of the righting reflex under thermal support. Soon after they were placed in sterilized cages containing sterilized surgical bedding. Post-operatively, the mice were placed on antibiotic feed for three days and the sutures were removed after seven day. Finally, the mice were monitored until the completion of the four weeks, at which point the animals were humanly euthanized for tissue collection via vaporized isoflurane (5%) in an induction chamber.

Table 2. List of treatment groups and type of implanted construct.

Treatment Groups	**Type of Implanted Construct**
Group #1	TIB-HMVECs
Group #2	TIB-βTC-6 cells
Group #3	TIB-HMVECs & βTC-6 cells
Group #4	Empty Construct (No cells)
Group #5	MP-HMVECs
Group #6	MP-βTC-6 cells
Group #7	MP-HMVECs & βTC-6 cells
Group #8	Empty Construct (No cells)

Histology

The harvested tissue samples were processed using a Spin Tissue Processor (Micro STP-120, Thermo Scientific). The dehydration process was performed by immersing tissue samples in different concentrations of ethanol (starting with 70%, 95%, 100%), followed by the clearing process where samples were immersed in xylene two times and finally infiltrated in paraffin. Paraffin embedded samples were then sectioned to 4 µm using a Sandon Finesse ® E/ME microtome. All samples were deparaffinized in three xylene washes then rehydrated in decreasing concentrations of ethanol (100%, 95%, 70%, 50%). Afterwards, tissue samples were stained with hematoxylin and eosin (H&E) staining.

3.5 Results and Discussion

Histology

Representative H&E stained tissue sections of the different excised constructs are shown in Figure 4. Figure 4A demonstrates the empty construct (control) with very few capillary-like structures within it. Interestingly, Figure 4B, the construct with TIB-ECs revealed a vast number of capillary-like structures as compared to the other treatment groups. The construct with MP-ECs on the other hand, had very few vessels in comparison (Figure 4C). Finally, the construct containing TIB-β-TC-6-C cells, Figure 4D, also shows very few vessels similar to the control group. A comparative analysis of all the eight treatment groups is displayed by a bar graph in Figure 5. As shown in the graph, TIB-ECs had the most growth of capillary-like structures and was significantly higher ($p = 0.009$) as compared to MP-ECs. We believe that this vast formation of vessels is possibly due to the heat and mechanical forces of the TIB process [36].

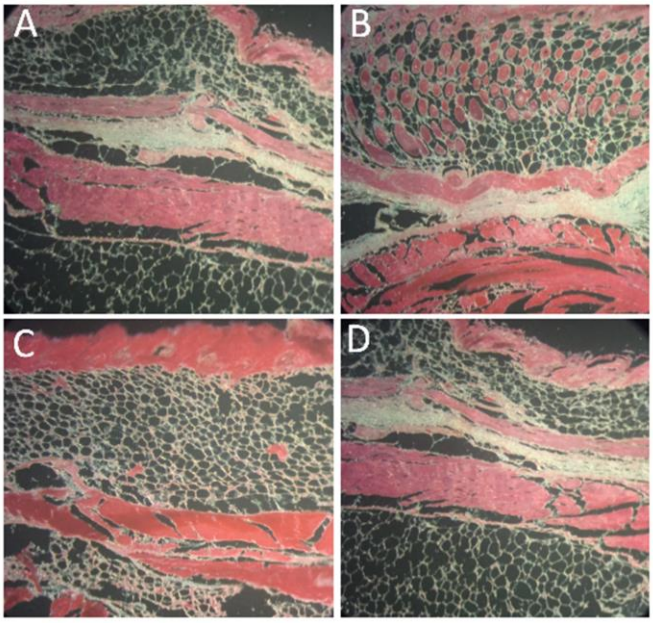

Figure 4. Histological analysis of excised subcutaneous tissue samples demonstrating the differences in capillary-like structures by treatment group.

A) The empty construct (control), demonstrated few capillary-like structures or vessels throughout the tissue section. **B)** TIB-EC construct, histological staining shows a high number of vessels at the implant site. **C**) MP-ECs implant, histological staining demonstrates a low number of vessels in and around the implant area. **D**) Beta-TC-6 implant showing few vessels similar to the control group.

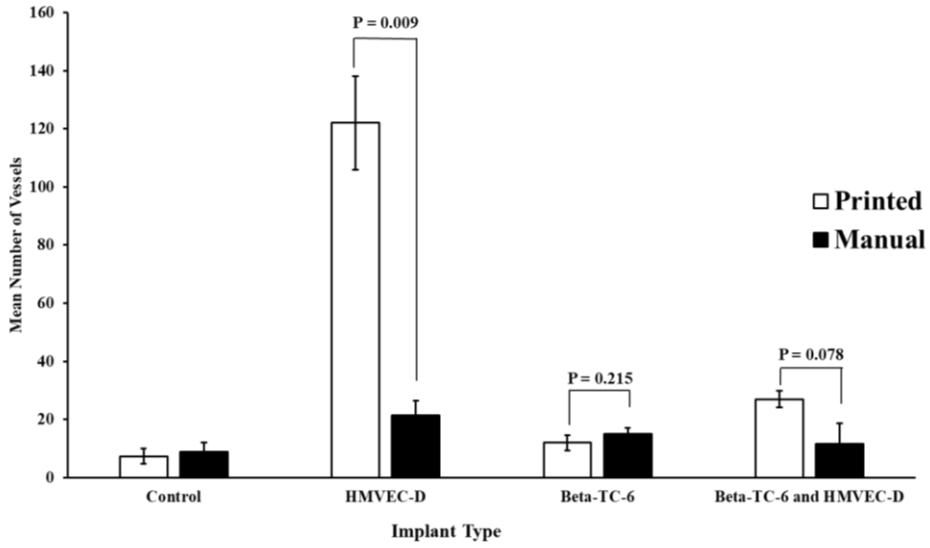

Figure 5. Bar graph demonstrating the mean number of vessels by implant type.

The bar graph demonstrates the mean number of vessels among the experimental groups while comparing constructs containing TIB-ECs and MP-ECs. Constructs with TIB-ECs had a significantly higher number of capillary-like structures as compared to constructs with MP-ECs at the end of 4 weeks ($p = 0.009$). HMVEC-D = Dermal human microvascular endothelial cells, Beta-TC-6 = pancreatic beta cells.

3.6 Conclusion

The histological results of our *in vivo* study showed a vast formation microvasculature among the excised bioengineered constructs containing TIB-ECs. These preliminary data provide compelling evidence that the TIB process is somehow inducing angiogenesis. Understanding the mechanism of how the TIB process causes the observed angiogenic transformation will help to fill a gap in knowledge about vascularization methods and potentially alter the wound dressing paradigm.

Chapter 4: TIB Elicits Morphological Changes, Cytokine Expression, and Kinase Activation *In Vitro*

4.1 Introduction

Bioprinters are advantageous in that they deposit cells and biomaterials in precise spatial arrangements to enhance cell-cell communication, decrease cell migration time in populating a tissue construct, and allow for the creation of artificial structures that closely resemble *in vivo* tissues and organs [37]. The three main types of bioprinters are inkjet, microextrusion, and laser-assisted printing. Comprehensive reviews on these bioprinters have been recently published [38][39][40][41][42]. Most, if not all of the printing modalities involve heat generation, be it via laser, heated nozzles, or friction as cells are forced through narrow orifices. Little is known, however, about the direct effects that bioprinting inflicts on cells. In Chapter 2, we demonstrated that TIB-ECs were recruited or otherwise involved in the formation of microvasculature in host animals [35][43]. Cross-species grafting markers such as stains that specifically stain for human cells nuclei were used to detect ECs in immunocompromised mice verified the connection of vascular structures between graft and host, also known as anastomoses [44]. Additionally, histological analysis of subcutaneous implants showed a significant higher number of capillary-like structures among constructs with TIB-ECs as compared to the controls.

While it is important to conduct studies that characterize the interaction between host and implanted bioprinted constructs, it is also important to understand the effects of the printing process in order to improve the engineering design of these tissues or to improve printer designs. Cells are fast adapting to their environment and they change intracellular structures, proliferation, movement, and differentiation in response to external mechanical stimuli [37][45]. In addition, changes in cell morphology due to mechanical injury may cause changes in downstream cellular development [37][46]. We hypothesize that the heat and mechanical forces experienced by the cells during the TIB process could have longer lasting effects on the cells ready to be transplanted. For these reasons, we sought to investigate whether TIB-ECs are being activated to secrete cytokines

in their supernatant and/or to phosphorylate kinases intracellularly. The heat or mechanical forces from the TIB process may cause HMVECs to release and activate specific angiogenic cytokines and kinases resulting in the vast formation of microvascular networks we observed. It has been demonstrated that HSP27 and other heat shock proteins regulate and induce angiogenesis, especially tumor angiogenesis [47][48]. Eighteen HSP90 inhibitors have recently entered the clinic as anti-cancer drugs [49], and HSP70 antagonists are explored as adjuvants [50]. However, in the field of tissue engineering and particularly bioprinting, the induction of angiogenesis via HSPs may be the desired response as vascularization and host integration of implants remains a considerable challenge.

4.2 Materials and Methods

Cell Culture: Primary adult human dermal microvascular endothelial cells (HMVECs) (Lonza) were cultured in EBM-2 media supplemented with an EGM-2 growth factor kit (Lonza) containing 10 ml FBS; 0.2 ml hydrocortisone; 0.2 ml hFGF-B; 0.5 ml VEGF; 0.5 ml R3-IGF-1; 0.5 ml ascorbic acid; 0.5 ml hEGF; 0.5 ml GA-1000; and 0.5 ml heparin. Cell cultures were maintained at 37 °C in a 5% CO_2 environment. Cells were passaged at 80% confluency and were used up to passage nine for the present experiments.

Bioink and Bioprinting Preparation: With the use of a thermal inkjet printer developed in our laboratory [51], a corresponding bioink solution was made with 0.13 M $CaCl_2$ in milli-Q water and sterilized via syringe filtration giving a final osmolality concentration of 300 mOsm/kg. HMVECs were trypsinized, counted, and mixed in the bioink solution to obtain a final concentration of 2 x 10^5 cells in 800 µl. One hundred microliters of the $CaCl_2$/HMVECs solution was loaded inside a modified printer cartridge and printed into the corresponding petri dish pre-filled with 6 ml of complete EBM-2 media.

Cell morphology analysis: Cell morphology of TIB and manually pipetted (MP) cells were observed using an Olympus IX71 at 10x (bright field) and 20x (phase contrast) after a 24-hour

incubation period. Images were taken with an Olympus DP72 digital camera with a 12.5 Megapixel resolution. Images were further processed on PowerPoint with a color tone of 6500 K, 100% color saturation, 0% brightness and contrast and a 50% sharpness.

Annexin V apoptosis analysis: An Annexin A5 fluorescein isothiocyanate (FITC)/propidium iodide (PI) Kit (Beckman Coulter) was used for detection of externalized phosphatidylserine (an early event of apoptosis induction) on TIB and MP cells after a 24-hour incubation period. HMVECs in complete media with 1 mM H_2O_2 used as positive control. Briefly, 2 x 10^5 cells were TIB and MP into 60 x 15 mm Petri dishes containing 6 ml of complete EBM-2/EGM2 media and incubated for 24 hours. After 24 hours, the supernatant with the floating dead cells was collected, the live attached cells were trypsinized, collected, and added to the initial supernatant containing the dead cells. Cells were washed with ice-cold 1X PBS and resuspended into a 106 µl from a 1060 µl master mix (1,000 µl binding buffer, 10 µl Annexin A5-FITC, and 50 µl PI) before a 15 minutes incubation in the dark. Finally, 300 µl of the kit's binding buffer was added to each tube and flow cytometric analysis was conducted within 30 minutes. Samples were analyzed in triplicates on a GALLIOS flow cytometer (Beckman Coulter). Debris was excluded by applying gates on side scatter vs. forward scatter histograms (data not shown). For all assays 10,000 events (cells) were acquired. The total percentage of apoptotic cells is demarcated as the sum of both early and late apoptotic subpopulations percentages; annexin V-FITC positive cells [52][53]. All flow cytometric data were analyzed using Kaluza software (Beckman Coulter).

Cell viability propidium iodide exclusion assay: HMVEC viability percentages were quantified in triplicates by a GALLIOS flow cytometer (Beckman Coulter) with the use of a propidium iodide (PI) exclusion assay [54][55]. Briefly, HMVECs were TIB and MP into a 6-well plate at a final seeding density of 40,000 cells/well in 6ml of EBM-2/EGM-2 complete media. Cell viability was then determined after a 3- and 7-day incubation period. At each incubation period, the supernatant containing all floating dead cells were collected. Live cells were then trypsinized and collected together with the initial supernatant. The complete cell samples were then stained with 5 µm/ml of PI, incubated for 15 minutes in the dark and analyzed *via* flow cytometry.

Unstained cells were used as controls to fine-tune the voltages for the FL1 and FL2 detectors, and to modify the compensation values resulting in a gated ovoid shape of living cells. For all assays, 10,000 events (cells) were acquired per sample and analyzed using the Kaluza software (Beckman Coulter).

Milliplex cytokine analysis: Multiplex magnetic bead immunoassays were performed on 0, 6, 12, and 24-hour supernatants collected from TIB and MP HMVECs from 60 x 15 ml Petri dishes containing 6 ml of complete media. HMVECs left in the $CaCl_2$ bioink for 1 hour at room temperature were used as a control and heat-shocked HMVECs passed through a Pasteur pipette heated with a soldering iron at 300 °C to mimic the bioprinting process were used as a negative control. Conditioned media was centrifuged for 5 minutes at 10,000 x g on a tabletop microcentrifuge at room temperature and divided into aliquots of 1.0 ml for storage at -4 °C until analysis. Supernatants were analyzed with the Milliplex Human Sepsis Panel 2 Magnetic Bead Panel with HSP70, IL-1α, and IL-8. Supernatants were also examined with the Milliplex Map Human Angiogenesis/Growth Factor Magnetic Bead Panel 1 with Ang-2, FGF-1, and VEGF-A (Millipore Sigma) according to the manufacturer's protocol with the use of the Luminex technology [56]. These six cytokines were selected due to their key angiogenic roles and their availability among the Milliplex magnetic bead panel products. Briefly, in a 96-well plate, 200 µl of Assay Buffer was added, the plate was shaken for 10 minutes, and the buffer was discarded. Twenty-five microliters of the standards, 25 µl of the Assay Buffer, 25 µl of stock solution, 25 µl of supernatant from cells into the corresponding wells, and 25 µl of the bead mixture were added. The plate was foil-wrapped and incubated overnight with shaking at 4 °C (Milliplex Human Sepsis Panel 2 was incubated for 2 hours at room temperature). The supernatant was removed and washed three times (washed twice for the Human Sepsis Panel 2) with 200 µl of wash buffer. Next, 25 µl of the detection antibodies were added, the plate was foil-wrapped, and incubated for 1 hour at room temperature with shaking. Without aspirating the supernatant, 25 µl of streptavidin-phycoerythrin was added, the plate was foil-wrapped, and incubated at room temperature for 30 minutes. The contents were discarded and washed three times (twice for the Human Sepsis Panel

2) with 200 µl of the wash buffer. Finally, 100 µl of the sheath fluid was added and the plate was read on a MAGPIX Instrument. Median fluorescent intensity (MFI) data using a 5-parameter curve-fitting method was used to measure analyte concentrations. The results from the samples were analyzed using the Luminex xPONENT Software Version 4.2 Build 1324.

Proteome phospho-kinase array: HMVECs from three T-75 flasks at ~80% confluency were TIB and manually (pipetted) seeded into a 100 x 15 mm Petri dish and incubated for 12 hours at 37 °C, 5% CO_2. Then, cells were washed with PBS, lysed in the presence of 1 mM phenylmethylsulfonyl fluoride, 5 µg/ml aprotinin, 2 µg/ml leupeptin, and 1 µg/ml pepstatin A proteases inhibitors and the resulting supernatant was clarified by centrifugation (14,000 x g, 5 minutes, 4 °C). Protein concentration was determined by the bicinchoninic acid method (Pierce). Equal concentrations of protein were analyzed using the Proteome Profiler Human Phospho-Kinase Array Kit (R&D Systems #ARY003B) according to the manufacturer's protocol. In this array, phosphorylation of 43 kinases and 2 related proteins were examined. Analytes and phosphorylation sites included: p38α (T180/Y182), extracellular signal regulated kinase 1/2 (ERK1/2) (T202/Y204, T185/Y187), jun N-terminal kinase 1/2/3 (JNK 1/2/3) (T183/Y185, T221/Y223), glycogen synthase kinase 3α/β (GSK-3α/β) (S21/S9), p53 (S392), epidermal growth factor receptor (EGF R) (Y1086), mitogen- and stress-activated protein kinase 1/2 (MSK1/2) (S376/S360), adenosine monophosphate-activated protein kinase α1 (AMPKα1) (T183), protein kinase B 1/2/3 (AKT 1/2/3) (S473), protein kinase 1/2/3 AKT 1/2/3 (T308), p53 (S46), mammalian target of rapamycin (mTOR) (S2448), cAMP response element-binding protein (CREB) (S133), heat-shock protein 27 (HSP27) (S78/S82), adenosine monophosphate-activated protein kinase α2 (AMPKα2) (T172), β-Catenin, p70 S6 Kinase (T389), p53 (S15), protein kinase c-Jun (c-Jun) (S63), protein kinase Src (Src) (Y419), protein kinase Lyn (Lyn) (Y397), protein kinase Lck (Lck) (Y394), signal transducer and activator of transcription protein 2 (STAT2) (Y689), signal transducer and activator of transcription protein 5a (STAT5a) (Y694), p70 S6 Kinase (T421/S424), ribosomal s6 kinase 1/2/3 (RSK1/2/3) (S380/S386/S377), endothelial nitric oxide synthase (eNOS) (S1177), protein kinase Fyn (Fyn) (Y420), protein kinase Yes (Yes) (Y426), protein

kinase Fgr (Fgr) (Y412), signal transducer and activator of transcription protein 6 (STAT6) (Y641), signal transducer and activator of transcription proteins 5b (STAT5b) (Y699), signal transducer and activator of transcription protein 3 (STAT3) (Y705), p27 (T198), phospholipase C-γ1 (PLC-γ1) (Y783), protein kinase Hck (Hck) (Y411), checkpoint kinase-2 (Chk-2) (T68), protein kinase FAK (FAK) (Y397), platelet-derived growth factor receptor β (PDGF Rβ) (Y751), signal transducer and activator of transcription protein a/b (STAT5a/b) (Y694/Y699), signal transducer and activator of transcription protein 3 (STAT3) (S727), lysine deficient protein kinase 1 (WNK1) (T60), proline-rich tyrosine kinase 2 (PYK2) (Y402), proline-rich AKT substrate (PRAS40) (T246), and heat-shock protein 60 (HSP60). Nitrocellulose membranes were visualized by enhanced chemiluminescence and X-ray film (Phenix). Densitometric analysis was performed using Image Studio Lite version 5.2.

Statistical analysis: All values are displayed as the average of triplicate, with their corresponding standard deviations. Statistical significance between two different samples was determined through two-tailed paired Student's *t*-tests, and a *P* value of less than 0.05 was considered statistically significant.

4.3 Results and Discussion

TIB-HMVECs demonstrate elongating characteristics: In order to determine distinguishing differences between TIB and MP cells, cell morphology between the two treatment groups was visualized. After a 24-hour incubation period, bright field microscopy images revealed that TIB-HMVECs demonstrate thin and long protuberances as compared to the MP-HMVECs (Figure 5). TIB-HMVECs are thin and elongated at 2-3 times longer than the MP. In both 10x and 20x images, one TIB-HMVEC is approximately 5-6 times the size of an MP-HMVEC (Figure 5(a) and (c)). Manually pipetted HMVECs, however, convey a thick, short, diamond-shaped body at both 10x and 20x magnification (Figure 5(b) and (d)). The elongation process among TIB cells might be due to the activation of these cells. Figure 9 illustrates that the TIB process had a

significant overexpression of VEGF-A and other angiogenic heat-shock proteins and cytokines as compared to MP cells. This response may be due to the heat and shear stress from the TIB process [57].

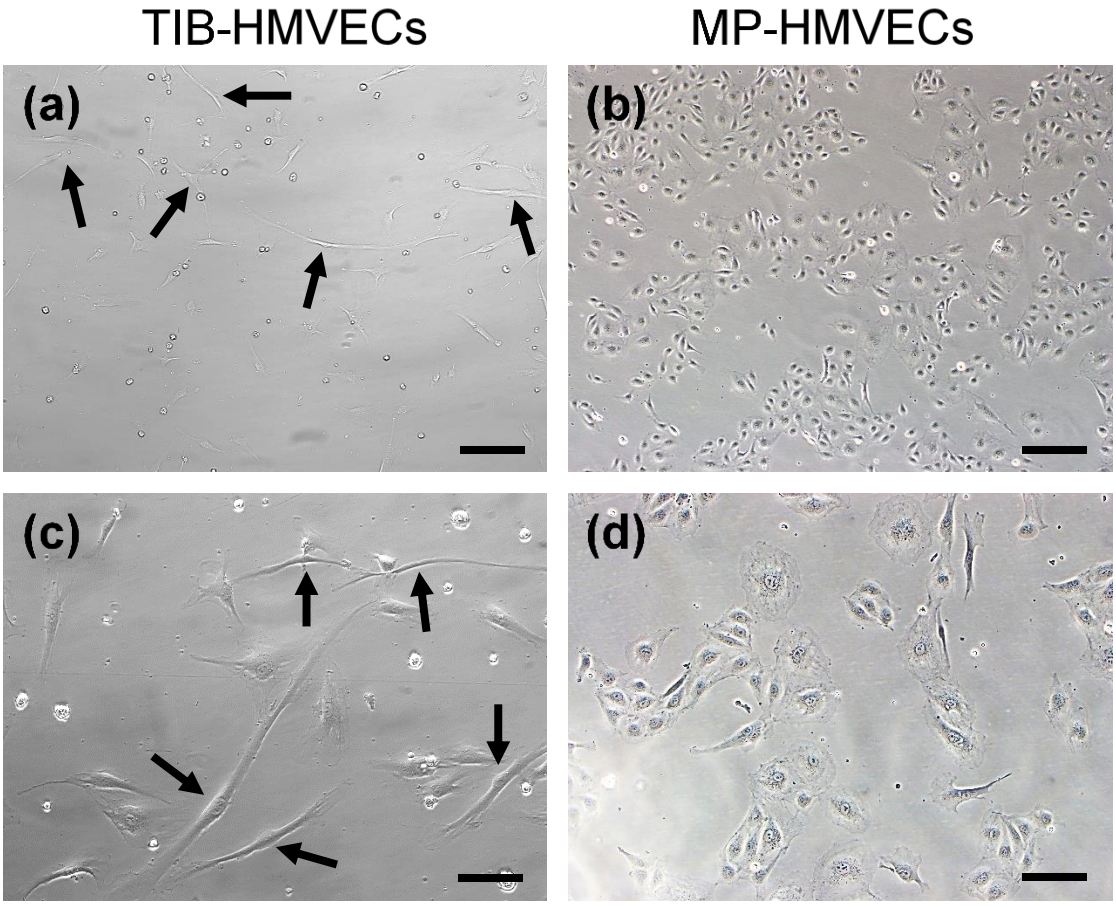

Figure 6. Cell morphology between TIB and MP HMVECs after a 24-hour incubation period.

(a) and **(c)** demonstrate TIB-HMVECs at 10x and 20x, respectively. Arrows indicate elongated cells. Images **(b)** and **(d)** show MP-HMVECs at 10x and 20x, respectively. Their appearance is almost diamond-shaped with some cells demonstrating minor elongation. TIB = thermal inkjet bioprinted. MP = manually pipetted, HMVECs = human microvascular endothelial cells, Scale bar 10x = 100 µm and 20x = 200 µm.

TIB induces cell apoptosis: To ensure that cells were viable after TIB, cell death was assessed by an apoptosis/necrosis protocol through the Annexin A5-FITC/PI assay analyzed via flow cytometry. In cells undergoing apoptosis, phosphatidylserine (PtdSer) is translocated to the outer leaflet of the plasma membrane facing the extracellular space [58][59][60][61]. Annexin, which has a high affinity for PtdSer, allows for the accurate detection of its externalization via flow

cytometry with the aid of FITC. A bar graph and the flow cytometer dot plots of the results are depicted in Figure 7. After a 24-hour incubation period, approximately 75% of TIB-HMVECs were apoptotic as compared to 22% of the MP cells (Figure 7(a), (b), and (c)). Note that HMVECs are very sensitive to manipulation and generally exhibit a lower viability than immortal/transformed cell lines (MP cells in Figure 7(a) and (c)). This sensitivity may be because these HMVECs are primary cells and thus short lived. However, in previous studies, TIB-Chinese Hamster Ovary (CHO) cells had a cell viability of 89% [57]. Additionally, the apoptotic percentages reported in Figure 7 were determined by the sum of the dead cells floating in the supernatant as well as the viable cells that were attached to the Petri dish after a 24-hour incubation period. Hydrogen peroxide (H_2O_2), which is a broadly effective inducer of apoptosis (depending on the concentration) [62], was used as a positive control and as expected, it resulted in a strong PtdSer externalization of 86% (Figure 7(d)). Apoptosis induction among TIB-HMVECs may seem relatively high, however, as noted in Figure 7(b), HMVECs are very sensitive primary cells resulting in a 67% viability with just trypsinizing and manipulation alone. Thus, findings suggest that the thermal inkjet bioprinting technology elicits apoptosis in HMVECs.

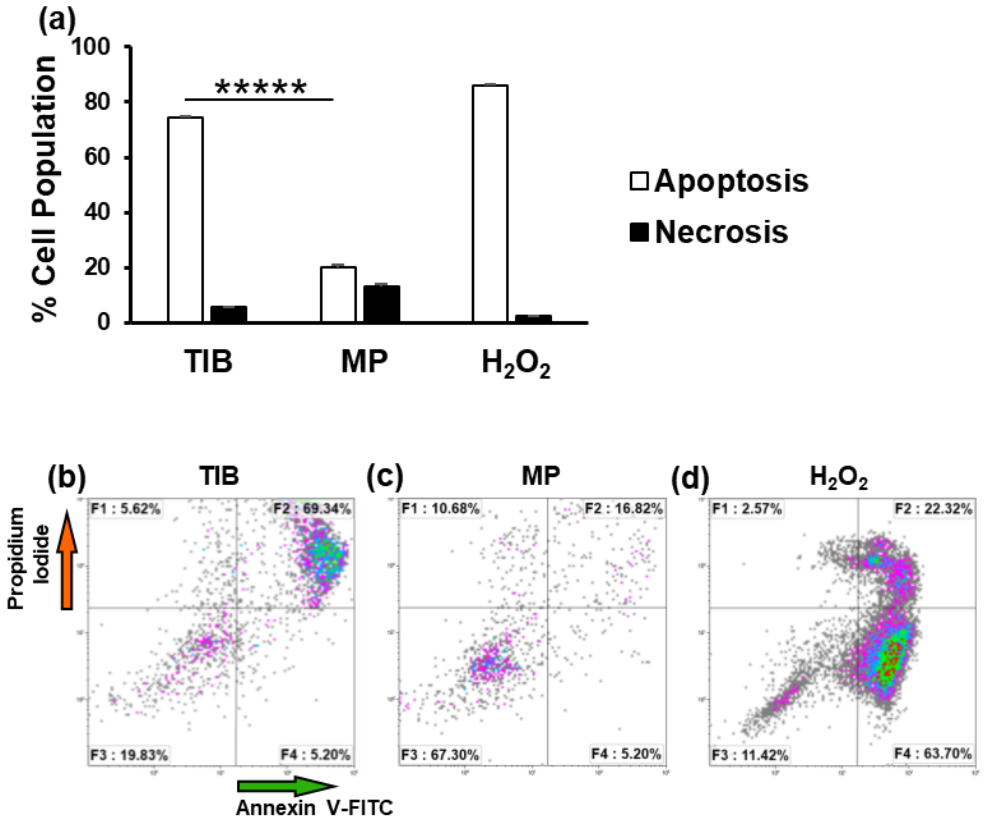

Figure 7. Flow cytometry analysis demonstrating phophatidylserine (PtdSer) externalization for TIB and MP HMVECs after a 24-hour incubation period.

F1 quadrant represents necrotic cells (PI positive and annexin negative). F2 quadrant represents cells that are in late apoptosis (both PI and annexin positive). F3 quadrant represents viable cells (both annexin and PI negative). F4 represents cells in early apoptosis (annexin positive and PI negative). **(a)** Bar graph demonstrating the differences in percentage rates of apoptosis and necrotic cells among TIB and MP HMVECs. The total percent of apoptotic cells is expressed as the sum of the early and late stages of apoptosis (white bars), as determined by the percentage of annexin V-FITC positive cells. Each bar represents the average of three independent measurements and the error bars represent their corresponding standard deviations. Dot plots show ratios of apoptosis among TIB-HMVECs. **(b)** Dot plots show ratios of apoptosis in TIB-HMVECs. **(c)** Dot plots show ratios of apoptosis in MP-HMVECs. **(d)** Dot plots show apoptosis of positive control (HMVECs in 1 mM H_2O_2). TIB = thermal inkjet bioprinted, MP = manually pipetted, HMVECs = human microvascular endothelial cells. *****$P < 0.00001$.

Effects of TIB on cell viability: Cell viability was measured after a 3 and 7-day incubation period with a PI exclusion assay and analyzed *via* flow cytometry. PI is impermeable to cells with intact cell membranes, however, in cells with ruptured membranes, the PI binds to the DNA rendering the dead cells highly fluorescent [63]. Displayed in Figure 8 are a bar graph and dot plots of the results. Figure 8(a) and (c) shows that after a 3-day incubation period, TIB-HMVEC's

viability was significantly higher in comparison to MP-HMVECs (92% vs 86% cell viability, respectively). After a 7-day incubation period, however, there was no significant difference in cell viability between TIB and MP cells, Figure 8(a) and (d). Figure 8(b) is a dot plot of untreated HMVECs without PI used as a control to determine the gate of viable cells. The reason we see a higher cell viability among TIB-HMVECs might be due to increased secretion of VEGF-A, Figure 10(c). VEGF is a potent mitogen that regulates endothelial cell proliferation [64][65]. At 7 days, these VEGF values might equilibrate to those similar to MP-HMVECs that we see in Figure 8(a) and (d). Overall, the high cell viability shown by TIB-HMVECs after a one-week incubation period demonstrates their potential incorporation into tissue engineering and regenerative medicine applications.

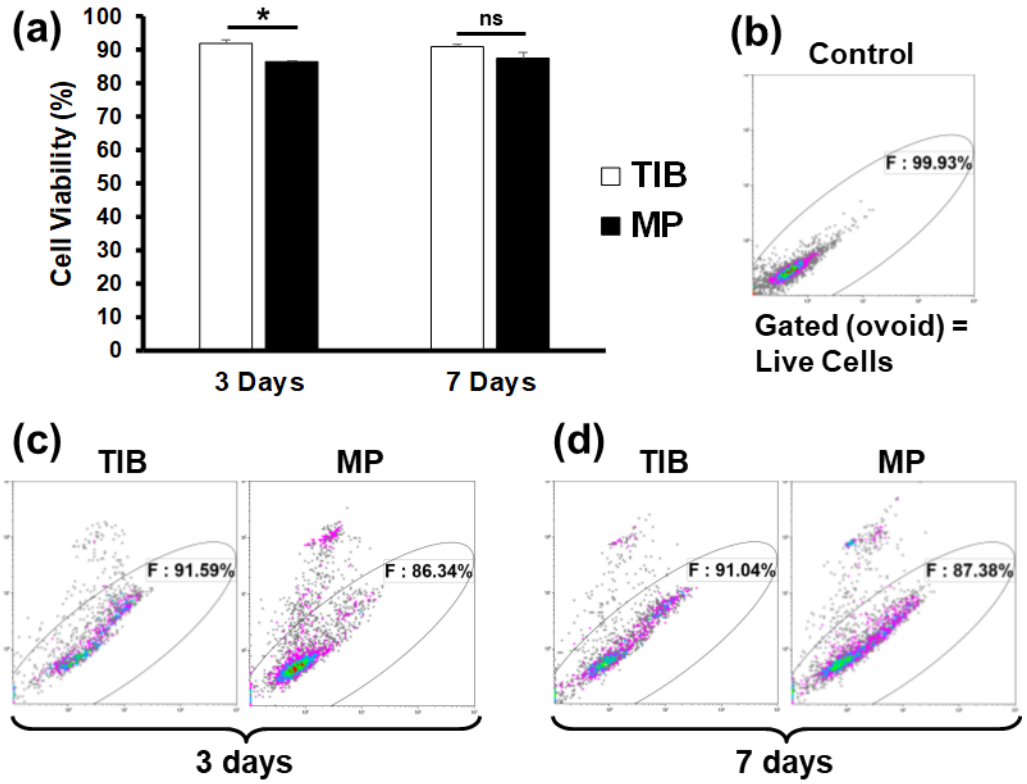

Figure 8. Flow cytometry analysis of a PI exclusion assay demonstrating cell viability percentages between TIB and MP-HMVECs at 3 and 7-day incubation periods.

(a) Bar graph depicting the differences in cell viability by percent among TIB and MP-HMVECs. Each bar represents the average of three independent measurements and the error bars represent their corresponding standard deviations. (b) Flow cytometric dot plot of untreated HMVECs without PI used to demark the gate of viable cells. (c) Dot plots demonstrating the differences in cell viability by percent between TIB and MP-HMVECs at a 3-day incubation period. (d) Dot plot showing the differences in cell viability by percent between TIB and MP-HMVECs at a 7-day incubation period. PI = propidium iodide, TIB = thermal inkjet bioprinted, MP = manually pipetted, HMVECs = human microvascular endothelial cells, ns = no significant difference. *P < 0.05.

TIB induces the expression of cytokines: The 6-panel multiplexed magnetic bead assay categorized the differences in cytokine expression between TIB and MP-HMVECs. Bar graphs in Figure 10 show the median fluorescent intensity (MFI) as it corresponds to the comparative expression levels of six specifically selected cytokines, including heat-shock protein 70 (HSP70), interleukin 1 (IL-1α), vascular endothelial growth factor A (VEGF-A), interleukin 8 (IL-8), fibroblast growth factor 1 (FGF-1), and angiopoietin 2 (Ang-2)**,** between TIB and MP-HMVECs. The MFI values for IL-1α and FGF-1 may appear low and insignificant in comparison to the other

four cytokines, however, when we took MFI readings of the EBM-2 media supplemented with an EGM-2 growth factor kit (Lonza), we found similar trends in their MFI values: IL-8, 12.5; IL-1α, 38.5; FGF-1, 106.75; Ang-2, 163; HSP70, 306; and VEGF-A, 6623. As noted, media alone (devoid of cells) contains great amounts of VEGF-A and low levels of IL-1α, IL-8, FGF-1, Ang-2, and HSP70. Interestingly, the amount of HSP70 found in the EMB-2/EGM-2 complete media alone was surpassed by over 7 times among TIB cells and was almost doubled in the MP cells. As a result, HSP70 was significantly overexpressed among TIB-HMVECs as compared to the MP cells (Figure 10(a)). This confirms that the TIB process is eliciting a heat shock response resulting in the production of HSP70. Additionally, IL-1α increased over three times the amount in media alone among TIB cells and increased slightly among MP cells with an overall significant overexpression between both treatment groups (Figure 10(b)). This further confirms the cell-based injury from TIB. IL-1α is a well-known inflammatory cytokine that is expressed in response to trauma [66]. Moreover, IL-1α has been shown to promote the production of HSP70 family proteins [67]. This also proves that pipetting cells manually causes minor cellular damage. The expression of VEGF-A in Figure 10(c) was more than doubled among TIB cells in comparison to their EBM-2/EGM-2 complete media values and may have been consumed by the MP cells. The observed VEGF-A expression may not only be due to the shear stress from the printing process [68], but also from the protective effects that HSP70 has on VEGF production. Kisher, A. et al., 2013, demonstrated that in cells recovering from heat shock, VEGF mRNA degradation decreased simultaneously as HSP70 expression levels increased [69]. Figure 10(d) shows the expression of IL-8 which was almost 700 times fold for TIB and over 400 times fold for MP cells in comparison to their complete media values. Furthermore, IL-8 was significantly overexpressed among TIB cells in comparison to MP cells.

Interleukin-8, another pro-angiogenic cytokine [67], increases proliferation, migration, and angiogenesis among ECs [70][71] by inducing VEGF secretion [72]. The expression of FGF-1 among TIB cells was similar to the value in the complete media, however, among MP cells, FGF-1 was completely depleted (Figure 10(e)). Also, FGF-1 was overexpressed significantly in TIB

cells in comparison to MP cells. Finally, the expression of Ang-2 among TIB cells was seven times the complete media values and over four times among the MP cells (Figure 10(f)). However, there were no significant differences in expression between both treatment groups. It may be possible that Ang-2 may have a synergistic effect with VEGF-A in our experiment [73][74]. It has been demonstrated that Ang-1 is the key angiopoietin in EC migration, survival, and vessel development and Ang-2 is its antagonist, however, along with VEGF, Ang-2 has proven to elicit angiogenic effects [75].

Altogether, another possible explanation for the observed effects could be due to the mechanical stretching of the cells as they are being bioprinted. As previously described in Figure 1, the mechanism behind the ejection of a bioink droplet is due to bursting or collapsing of bubbles formed by a heating element inside the cartridge. As can be seen from Figure 2, the ejected drops are oblong in shape with very long tails compared to their diameter. As the drops are ejected through the air, the surface tension of the liquid tends to pull the tails back into the main drop. Sometimes the tails are pinched off and small satellite drops are formed. It is possible that when the cells are mixed within this liquid phase, their membranes will be stretched if they are on the tail region of the drop. If the pinching occurs, the membrane will rupture, and cell will die. We attribute the cell death seen in our results to this pinching off and satellite drop formation. Cells that are largely in the bulk of the drop, may only experience some stretching of their membranes due to the tail. One would expect many of these to survive but having somewhat leaky membranes at first.

According to Cui X. et al., 2010 who performed cell damage evaluation on TIB Chinese hamster ovary (CHO) cells, transient cell membrane pores were created among TIB-CHO cells. By averaging the Stokes diameters of dextran molecules that penetrated CHO cell membranes, they estimated that the average pore size was 105 Å at 25 minutes after being TIB, then 37 Å after one hour, and eventually disappeared at two hours [57]. The formation of these pores might possibly due to the stretching of their cell membranes. According to Pedrigi, R.M. et al., 2017, ECs are extremely sensitive to mechanical stimulation and numerous studies have demonstrated

that shear stress and stretching have activated the expression of proliferation, migration, and angiogenic mediators [76]. Similarly, Jufri, N.F. et al., 2015, found HSP70, VEGF, FGF, PDGF, and Ang-2 expression due to mechanical stretching of ECs [77], further supporting our findings. Thus, although these cells are exposed to a heating element that heats up to 300 °C, the actual temperature of the bioink is approximately 4-10 °C degrees above ambient temperature [31][6] or around 46°C [57] and lasts for about 10 μs before the cell is ejected [78], we firmly believe that the reason for our observed results is due to the mechanical forces that causes EC stretching as they are being bioprinted [79].

In a previous experiment, cytokine expression was assessed at 0, 6, 12, and 24-hour periods and found that the most VEGF-A, IL-8 and FGF-1 expression occurred at 12 hours. For this reason, the 12-hour incubation period was chosen for the present experiment. Figure 4 demonstrates the differences of expression among the six afore mentioned cytokines consisting of TIB, MP, cells left in bioink (Bioink), and heat shocked (HS) cells within a 24-hour time course period. To test if the $CaCl_2$ bioink had any effect on the expression of these cytokines, a control group consisting of HMVECs left in the bioink for an hour at room temperature was examined. As expected, minimal values of cytokine expression were lower than their EBM-2/EGM-2 complete media (Figure 9(a)-(f)). Additionally, to examine if cell contents from ruptured HMVECs were releasing vast amounts of the selected cytokines, a negative control consisting of heat shocked HMVECs ejected from a Pasteur pipette heated with a solder iron to 300 ºC resulting in complete cell death was included. Once again, minimal values of cytokine expression were detected in comparison to their EBM-2/EGM-2 complete media (Figure 9(a)-(f)). This test proved that cytokine expression is an active and not a passive process.

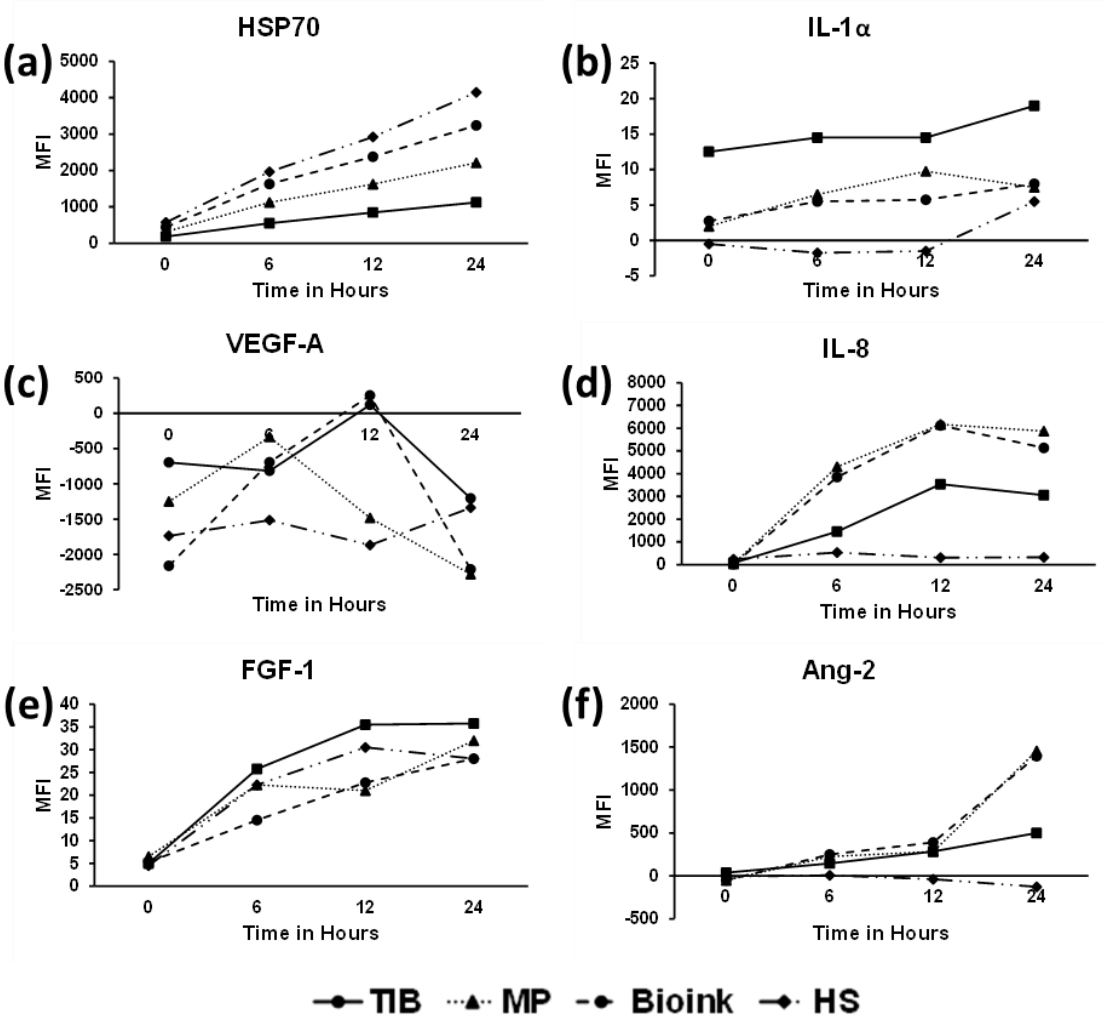

Figure 9. Time course expression of six specifically selected cytokines by treatment group.

(a) HSP70 demonstrated increased expression with time, with HS cells having the most expression. **(b)** IL-1a demonstrated a steady expression with time and was most noticeable among TIB cells. **(c)** VEGF-A showed the most expression at 12 hours by MP and TIB cells. **(d)** IL-8 expression peaked at 12 hours and decreased slightly at 24 hours among MP, Bioink, and TIB cells. **(e)** FGF-1 expression peaked at 12 hours and plateaued afterwards for TIB cells. **(f)** Ang-2 was expression was most noticeable at 24 hours among MP and Bioink cells.

We are confident that the TIB process activates or promotes angiogenic signals in HMVECs. We purposely selected these six cytokines due to their potent angiogenic effects. HSP70-1A, a member of the HSP70 family, binds to the surface of endothelial cells (ECs), activates HUVEC migration and tube formation *in vitro***,** and promotes vascularity formation *in vivo* [80]**,** and is required for IL-5 induced angiogenic responses [81]. FGF-1 regulates cell differentiation, proliferation, survival, and angiogenesis [82]. To date, VEGF-A is the most potent

pro-angiogenic cytokine. It promotes proliferation, tube formation, and sprouting of ECs [83][84]. Our TIB process did induce the expression of six potent angiogenic cytokines and these may be the reason behind the differences in morphological differences between the TIB and MP-HMVECs as depicted in Figure 6.

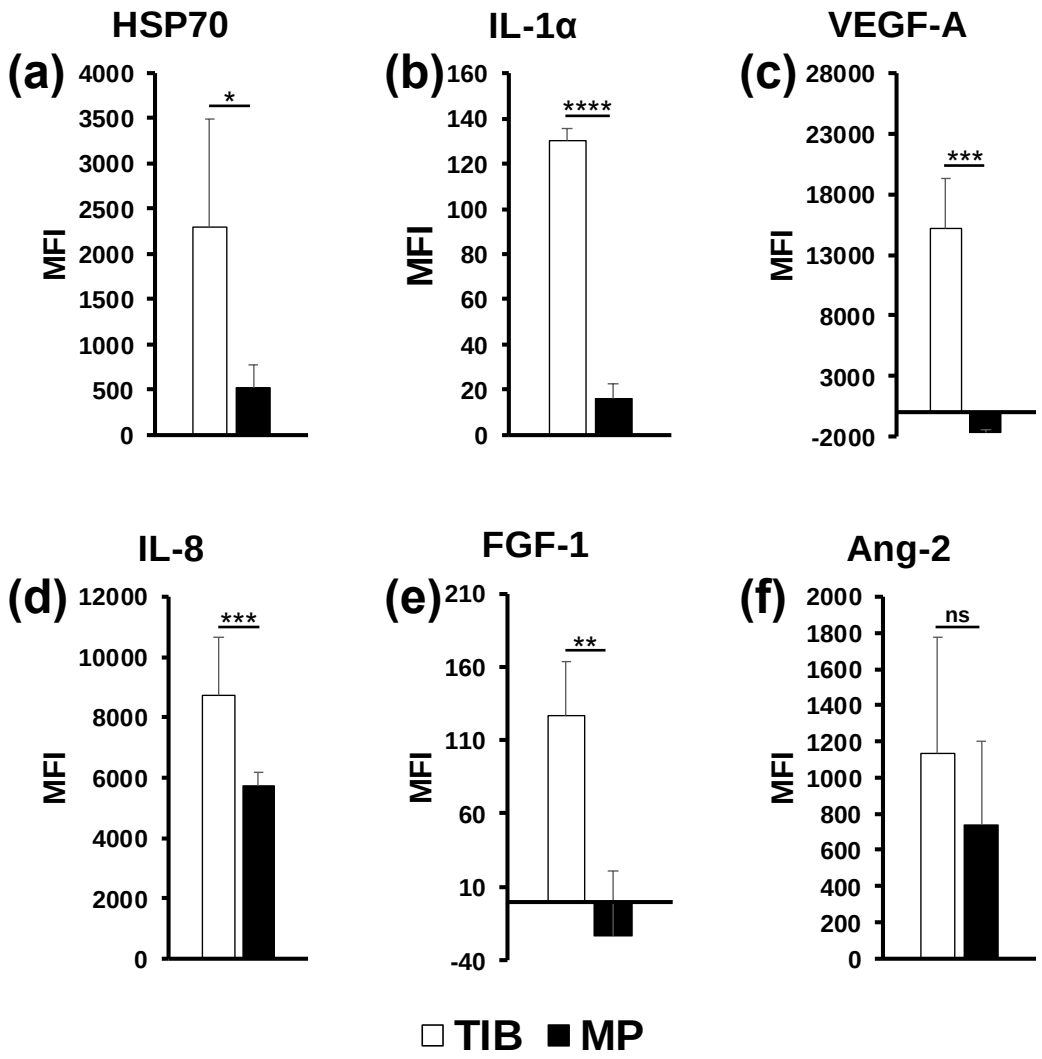

Figure 10. In vitro Milliplex magnetic bead panel analysis of six specifically selected cytokines after a 12-hour incubation period.

(a) HSP70 was significantly overexpressed in TIB-HMVECs as compared to MP-HMVECs. **(b)** IL-1α was significantly overexpressed among TIB-HMVECs in comparison to MP-HMVECs. **(c)** VEGF-A was significantly overexpressed in TIB-HMVECs as compared to MP-HMVECs. **(d)** IL-8 was significantly overexpressed in TIB-HMVECs as compared to MP-HMVECs. **(e)** FGF-1 was significantly overexpressed among TIB-HMVECs in comparison to MP-HMVECs. **(f)** Ang-2 demonstrated no significant differences in expression between TIB and MP-HMVECs. HSP70 = heat shock protein 70, IL-1α = interleukin 1α, VEGF-A = vascular endothelial growth factor A, IL-8 = interleukin 8, FGF-1 = fibroblast growth factor 1, Ang-2 = Angiopoietin 2, TIB = thermal inkjet bioprinted, MP = manually pipetted, HMVECs = human microvascular endothelial cells, MFI = median fluorescent intensity, ns = no significant difference. *$P < 0.05$; **$P < 0.01$; ***$P < 0.001$; ****$P < 0.0001$.

TIB activates the phosphorylation of kinases: To determine the molecular mechanism by which TIB activates HMVECs, we performed a proteome phospho-kinase array of 43 kinases and

two proteins. The bar graph depicted in Figure 11(a) demonstrates that STAT3, Fyn, mTOR, and AKT1/2/3 were significantly under activated in TIB cells as compared to MP cells. Similarly, the bar graph in Figure 11(b), shows that Yes, CREB, Src, Chk2, AMPKα1, c-Jun, FAK, GSK-3α/β, JNK1/2/3 were under activated significantly in TIB-ECs as compared to the MP cells.

Grouped together, the non-receptor tyrosine kinases Fyn, Yes, Src, and FAK are involved in survival, proliferation, migration, and angiogenesis [85][86][87]. Similarly, the serine/threonine kinases, AKT1/2/3, mTOR, GSK-3α/β, and JNK1/2/3, are also involved in the regulation of apoptosis, survival, proliferation, migration, angiogenesis [88][89][90][91], cellular homeostasis (AMPKα1/2) [92], and a cell division checkpoint (Chk2) [93]. Finally, the CREB, c-JUN, and STAT3 transcription factors are also involved in survival, proliferation, and angiogenesis [94][95][87]. The grouping of each type of kinase, protein, transcription factor, and heat shock protein are listed in Table 3 along with their individual function. Additionally, Figure 12 depicts an illustration detailing where the kinases and proteins play a role among the different signaling pathways. Altogether, our findings suggest that TIB-ECs were not proliferating as compared to the MP cells. Possibly, TIB-ECs have an entered a nonproliferative state due to a state of shock after the harsh TIB process which resulted in a 25% viability as seen in Figure 7. Perhaps growth-arrest genes were activated due to the mechanical stretching stress induced by the TIB process. This is further supported by Chien, S., (2007) who confirmed that ECs under the effects of shear stress demonstrated a nonproliferaive state as compared to cells without shear stress *in vitro* [96].

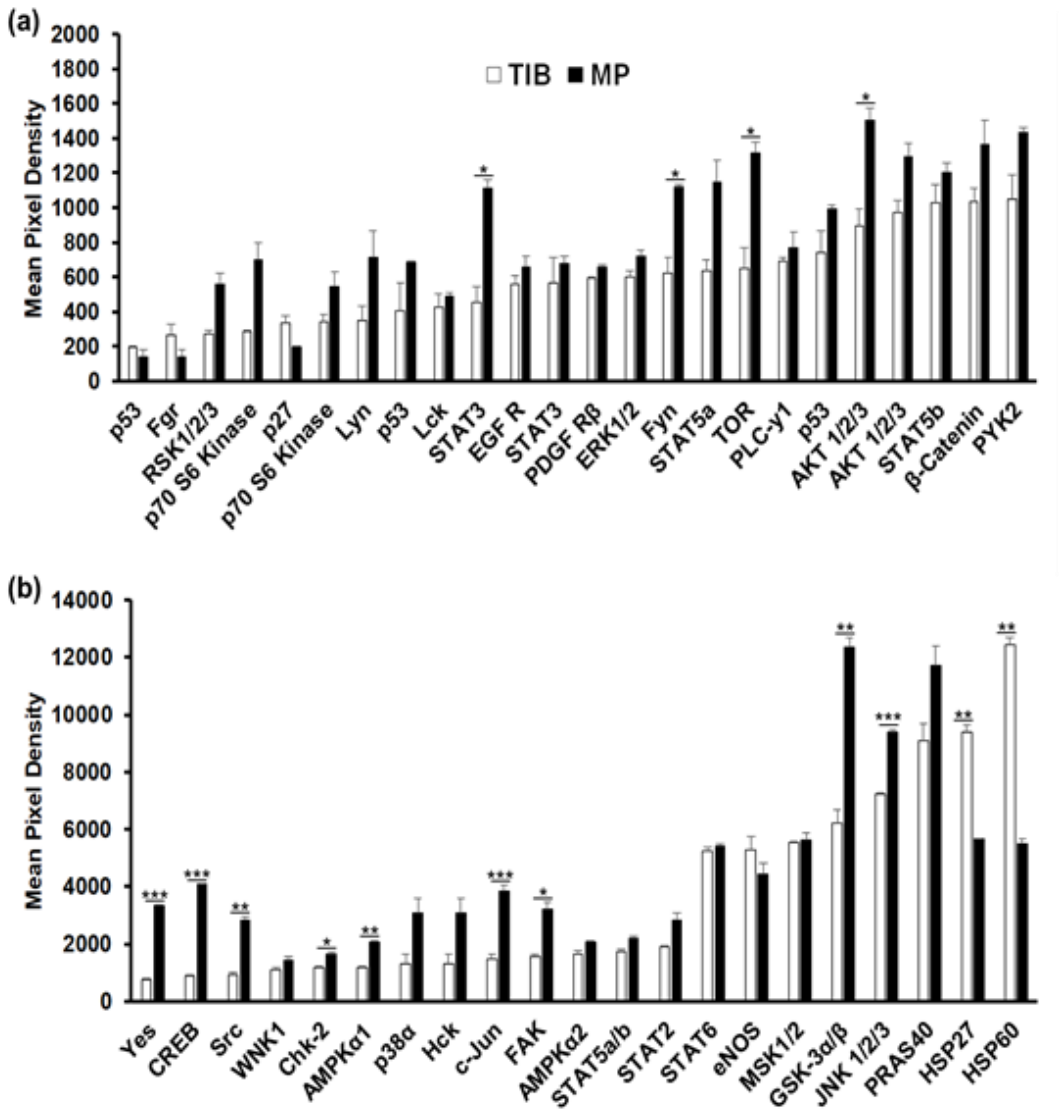

Figure 11. In vitro Human phosphor-kinase array analysis of the activation of 43 kinases and two proteins after a 12-hour incubation period.

(a) STAT3, Fyn, TOR, AKT 1/2/3 were significantly overactivated among MP-HMVECs as compared to TIB-HMVECs.(b) Yes, CREB, Src, Chk-2, AMPKα1, c-JUN, FAK, GSK-3α/β, and JNK 1/2/3 were significantly overactivated among MP-HMVECs as compared to TIB-HIMVECs while HSP27 and HSP60 were overactivated significantly in TIB-HMVECs in comparison MP-HMVECs. STAT = signal transducer and activator of transcription proteins, EGF R = epidermal growth factor receptor, PDGF R = platelet-derived growth factor receptor, AKT = protein kinase B, PYK-2 = proline-rich tyrosine kinase 2, CREB = cAMP response element-binding protein, WNK1 = lysine deficient protein kinase 1, AMPK = adenosine monophosphate-activated protein kinase, eNOS = endothelial nitric oxide synthase, MSK = mitogen- and stress-activated protein kinase, GSK = glycogen synthase kinase, JNK = Jun N-terminal kinase, PRAS = proline-rich AKT substrate, HSP = heat-shock protein, TIB = thermal inkjet bioprinted, MP = manually pipetted, HMVECs = human microvascular endothelial cells. *P < 0.05; **P < 0.01; ***P < 0.001.

Furthermore, TIB-ECs showed a significant over activation of HSP27 and HSP60 as compared to MP cells, Figure 11 (b). Interestingly, both of these HSPs have been proven to play angiogenic roles [97] and have been demonstrated to be activated by mechanical stretching [98][99]. It is well established that the nuclear factor kappa-light-chain enhancer of activated B cells (NF-κB) activation from HSP27 leads to the secretion of IL-8 and VEGF [100]. Moreover, HSP27 actives toll-like receptors (TLRs) on ECs to induce NF-kB activation, resulting in VEGF-mediated EC migration and angiogenesis [101]. Similarly, HSP60 has also been shown to promote angiogenesis [102]. HSP60 has been shown to be localized in the mitochondria of unstressed HUVECs, however, in stressed HUVECs, HSP60 was found in the cytoplasm and surface membrane [103].

Table 3. List of kinases and proteins by category and function.

Serine/Threonine Kinases	**Functions**
AKT 1/2/3	Apoptosis regulation, survival, proliferation, migration, angiogenesis, activated by mechanical stimuli, shear stress, heat, and VEGF. Involved in AMPK, mTOR, NF-kB, PI3K/Akt, and PKC signaling. p70S6K involvement
AMPKα1/2	Energy sensor activated with low ATP levels. Inhibits lipid, protein, carbohydrates production. Inhibits cell growth and proliferation. AMPK, insulin receptor, and mTOR signaling
Chk2	Apoptosis regulation, proliferation G1/S checkpoint, G2/M DNA damage checkpoint
ERK 1/2	Apoptosis, survival, angiogenesis, response to mechanical stimuli, growth and differentiation by MAPKs. mTOR signaling, P70S6K involvement
GSK-3 α/β	Survival, proliferation, angiogenesis, activated by heat, growth and differentiation by MAPKs. mTOR, PI3K/Akt, NF-kB, Wnt/β-Catenin signaling. P70S6K involvement
JNK 1/2/3	Apoptosis regulation, survival, proliferation, migration, angiogenesis, activated by mechanical stimuli. NF-kB, SAPK/JNK, and Toll-Like Receptor signaling.
MSK 1/2	Survival, proliferation, growth and differentiation by MAPKs. NF-kB signaling, P38 MAPKs regulation
P27	Regulator of cell cycle progression, inhibits CDK2 activity, growth and differentiation by MAPKs, PI3K/Akt signaling
P38α	Survival, proliferation, VEGF stimulus, angiogenesis, inflammation, activated by heat. NF-kB, PLC, and Toll-Like

	Receptor signaling, P38 MAPKs regulation, p70S6K involvement
p70S6K	Survival, proliferation, angiogenesis. AMPK, mTOR, PI3K/Akt, and PLC signaling
RSK 1/2/3	Survival, proliferation, GPCR signaling to MAPKs, growth and differentiation by MAPKs, mTOR and Toll-Like Receptor signaling. p70S6K involvement
WNK-1	Electrolyte homeostasis, survival, proliferation
Phosphatidylinositol 3-Kinase related Kinase	**Functions**
mTOR	Survival, metabolism, proliferation, migration, stress signals, angiogenesis. AMPK, mTOR, and PI3K/Akt signaling. p70S6K involvement
Proteins	**Functions**
β-Catenin	Cell adhesion, regulation of FGFR, NF-kB, and MAPK signaling, regulation of angiogenesis, Wnt/βCatenin signaling
eNOS	Angiogenesis, migration, AMPK and PI3K/Akt signaling
PLCγ-1	Migration, angiogenesis, growth and differentiation by MAPKs, phospholipase signaling. Activation by PDGFR, FGFR, EGFR
PRAS40	Subunit of mTOR, survival, mTOR and PI3K/Akt signaling. p70S6K involvement
Transcription Factors	**Functions**
c-JUN	Apoptosis regulation, proliferation, angiogenesis. SAPK/JNK signaling
CREB	Survival, proliferation, angiogenesis, growth and differentiation by MAPKs, activation by PDGF, and P38 MAPKs regulation
p53	Apoptosis regulation, proliferation, tumor suppressor, DNA damage stimulus. AMPK, PI3K/Akt, SAPK/JNK signaling, G1/S and G2/M checkpoints, P38 MAPKs regulation
STAT1	Survival, inhibition of angiogenesis, endothelial cell proliferation, and NF-kB signaling. JAK/STAT signaling
STAT2	Viral response, IFNa/b activation, JAK/STAT signaling
STAT3	Survival, proliferation, inflammation, angiogenesis, growth and differentiation by MAPKs. SAPK/JNK, NF-kB, and JAK/STAT signaling
STAT5a/b	Endothelial cell proliferation and migration, activation via FGFR, JAK/STAT signaling
STAT6	Mammary gland morphogenesis, JAK/STAT signaling
Receptor Tyrosine Kinases	**Functions**
EGFR	Angiogenesis, proliferation, migration, activated by mechanical stimuli. PLC signaling
PDGFR	Proliferation, migration, angiogenesis. MAPKs and PI3K/Akt signaling. Activates STAT1, STAT3, and STAT5A/B

Non-Receptor Tyrosine Kinases	Functions
FAK	Actin cytoskeleton, proliferation, migration, angiogenesis, GPCR signaling to MAPKs, growth and differentiation by MAPKs, PI3K/Akt signaling
Fgr	Src family, found in hematopoietic cells, immune response, PI3K activity, cytokine secretion. GPCR signaling to MAPKs
Fyn	Src family, actin remodeling, survival, proliferation, migration. GPCR, growth and differentiation signaling by MAPKs
Hck	Src family, found on hematopoietic cells, survival, proliferation, cell adhesion, migration, GPCR signaling to MAPKs
Lck	Src family, T-cell selection, maturation, and function in thymus. GPCR signaling to MAPKs
Lyn	Src family, proliferation, migration, B-cell homeostasis. GPCR signaling to MAPKs and PI3K/Akt signaling
Pyk2	FAK family, actin cytoskeleton, polarization, adhesion, proliferation, migration, angiogenesis, response to mechanical stimuli and shear stress, GPCR signaling to MAPKs, growth and differentiation by MAPKs, PI3K/Akt signaling
Src	Actin and microtubule dynamics, survival, proliferation, migration, angiogenesis, immune response, GPCR signaling to MAPKs, growth and differentiation by MAPKs, Wnt/β-Catenin signaling
Yes	Survival, apoptosis regulation, cell adhesion, cytoskeleton remodeling, migration, activated by EGFR, PDGFR, FGFR. GPCR signaling to MAPKs
Heat-Shock Proteins	**Functions**
HSP27	Chaperone, survival, angiogenesis via VEGFR cascade and VEGF mediated migration. P38 MAPKs regulation
HSP60	Chaperonin, apoptosis via mitochondria, B and T cell activity, MyD88-dependent Toll-like receptor cascade

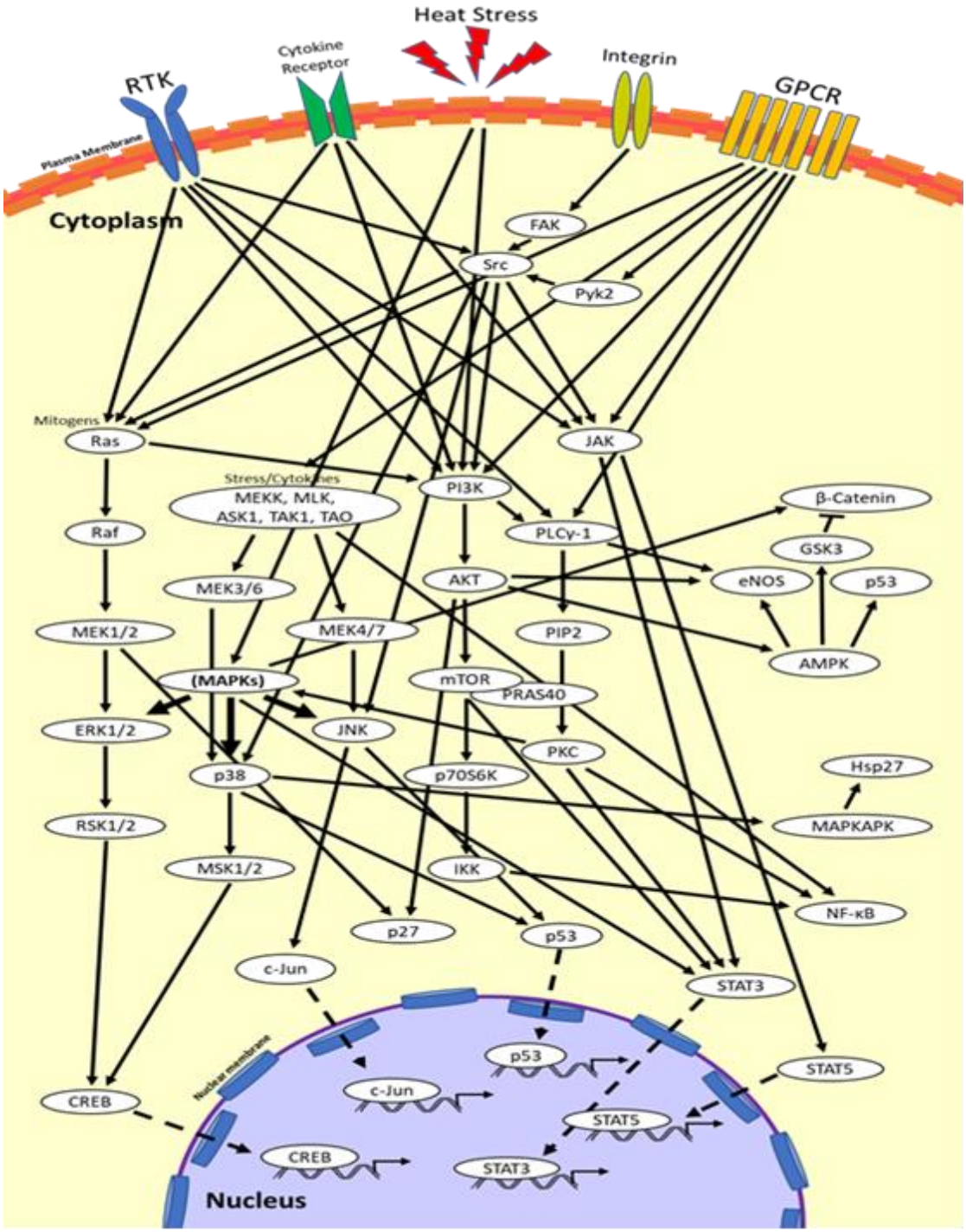

Figure 12. Molecular mechanisms involved in RTK, cytokine receptor, heat stress, integrin, and GPCR signaling.

Simplified schematic of the signaling pathways involved in the activation of the CREB, c-JUN, p53, STAT3, and STAT 5 transcription factors activated by a(n) RTK, cytokine receptor, heat stress signal, integrin, and GPCR. CREB = Cyclin amp Response Element-Binding Protein, STAT = Signal Transducer and Activator of Transcription, RTK = Receptor Tyrosine Kinase, GPCR = G-Protein Coupled Receptor.

The effects observed in our study may not only be specific to thermal inkjet printers but might also occur in laser-based direct-write printing, electrospinning techniques for cell patterning and possibly extrusion-based systems when small diameter nozzles are used. Laser-based direct-write printing technologies include laser-induced forward transfer (LIFT), absorbing film-assisted laser-induced forward transfer (AFA-LIFT), biological laser processing (BioLP), matrix-assisted pulsed laser evaporation direct writing (MAPLE DW), and laser-guided direct writing (LG DW) [104]. Cell electrospinning consists of electrospun cell-laden threads within a specific biosuspension [105]. In laser-based direct-write cell patterning, the laser heats the laser absorption layer, causing the formation of a bubble which collapses, resulting in the specified pattern. Cell viability regarding cell acceleration and deceleration as the cell droplet forms and lands on the substrate is discussed. However, there is no mention of the heat stress induced by the laser [104]. Regarding cell electrospinning, cell viability was found to be 25%, similar to other findings [106]. Among solid freeform fabrication-based direct cell writing, dispensing pressure and nozzle size was found to induce mechanical cell membrane damage [37].

As we have documented, all these different cell manipulations or patterning techniques for the purposes of biofabricating living systems induce some form of stress or significant cell death. For this reason, we ought to characterize the expression and activation of various cytokines and kinases among other biofabrication techniques to see if we are indeed creating the desired effects upon implantation. There is also the possibility that the bioprinting process changes the intracellular structures of the cells**,** leading to the physiological change of cells and possibly inducing cell transformation or uncontrolled cell growth. In this case, the focus towards new biofabricating modalities should involve designing novel cell manipulation techniques that promote less heat and mechanical induced cellular trauma. Enlarging nozzle sizes or cell encapsulating methods could also be implemented in order to minimize the downstream damaging effects from the bioprinting process.

4.4 Conclusion

In conclusion, we have demonstrated that TIB-ECs significantly overexpressed five angiogenic cytokines and significantly over activated two HSPs that also play an angiogenic role. Moreover, due to these observations and our supporting evidence, we now firmly believe that as ECs are being ejected from the nozzles, they are being stretched out among the tails of the droplets. In doing so, they become activated by a mechanical stress rather than a heat-stress as we previously hypothesized. It is hoped that with further progress, our TIB technology could be used as a new vascularization strategy since the formation of anastomosis and functional vascular networks remains a tremendous challenge in the field of tissue engineering and regenerative medicine [107].

Chapter 5: Conclusions, Limitations, and Future Work

Conclusions

In conclusion, we have demonstrated that constructs containing TIB-ECs offers an alternative method to inducing microvascular networks in vivo. Our *in vitro* data also supports our findings as they translate *in vivo*. In a recent separate *in vivo* study, performed on humanized mice, while following the same protocol exhibited similar results to those we obtained (manuscript in progress). Similarly, our *in vitro* observations also uphold our hypothesis that ECs are exposed to mechanical stress inside the reservoir of the cartridge resulting in the stretching of these cells as they are being bioprinted. The ability to create vast capillary networks, coupled with the fixed printing parameters of our TIB technology (i.e. heat, pressure, nozzle size, droplet size, and velocity) allows for versatile and repeatable means to create these constructs.

Limitations

A major limitation of this work mainly rested on the clogging of the modified printer cartridges during the bioprinting process. We believe that the channels leading to the nozzles become blocked by cellular sedimentation as well as cellular debris from the harsh heat and mechanical forces associated with bioprinting. As a result, multiple to cartridges are needed to carry out experiments, especially those that require a vast number of cells, such as the proteome phosphorylation kinase array previously presented. Additionally, even though desktop inkjet printers are still widely accessible, the original ink cartridges are difficult to acquire. The original cartridges have become obsolete and are no longer in production. Among the original cartridges we managed to purchase, we have observed corrosion of the outer electrical components due to the ink that leaked during years of storage. Printing using replica cartridges was also limited as they ejected few to no cells following the initial print. Efforts to unclog the few cartridges on hand

include the use of sonication, forced pressure ejection (using a syringe), and boiling as well as acetic acid, EDTA, and trypsin solutions. These methods have demonstrated some efficacy and provide temporary use, but ultimately, they stop printing. Presently, the issue of cartridge restoration continues to limit its bioprinting capacity.

Future Work

Future *in vitro* work with appropriate controls for mechanical stress or possibly printing with the cartridge submerged within media to control for cellular stretching are recommended. Also, *in vivo* work with diabetic or impaired wound healing models such as a diabetic foot ulcer along with the afore mentioned controls are also suggested. Additionally, a comparative study among different types of commercially available ECs and/or TIB modalities are also recommended. Looking ahead, bioengineered constructs using our TIB technology may find potential applications in organ on a chip, drug testing, and autonomic healing applications.

References

[1] L. Yazdanpanah, M. Nasiri, and S. Adarvishi, "Literature review on the management of diabetic foot ulcer.," *World journal of diabetes*, vol. 6, no. 1. pp. 37–53, 2015.

[2] W. Clayton and T. A. Elasy, "A Review of the Pathophysiology, Classification, and Treatment of Foot Ulcers in Diabetic Patients," *Clin. Diabetes*, vol. 27, no. 2, pp. 52–58, 2009.

[3] T. Emanuelli, A. Burgeiro, and E. Carvalho, "Effects of insulin on the skin: possible healing benefits for diabetic foot ulcers," *Archives of Dermatological Research*, vol. 308, no. 10. pp. 677–694, 2016.

[4] T. Dinh, F. Tecilazich, A. Kafanas, J. Doupis, C. Gnardellis, E. Leal, A. Tellechea, L. Pradhan, T. E. Lyons, J. M. Giurini, and A. Veves, "Mechanisms involved in the development and healing of diabetic foot ulceration," *Diabetes*, vol. 61, no. 11, pp. 2937–2947, 2012.

[5] W. D. Aumiller and H. A. Dollahite, "Pathogenesis and management of diabetic foot ulcers," *J. Am. Acad. Physician Assist.*, vol. 28, no. 5, pp. 28–34, 2015.

[6] X. Cui, T. Boland, D. D. D'Lima, and M. K. Lotz, "Thermal inkjet printing in tissue engineering and regenerative medicine.," *Recent Pat. Drug Deliv. Formul.*, vol. 6, no. 2, pp. 149–55, 2012.

[7] F. J. Alvaro-afonso, "Advances in dermoepidermal skin substitutes for diabetic foot ulcers Advances in Dermoepidermal Skin Substitutes for Diabetic Foot Ulcers," no. April, 2019.

[8] G. Messenger, R. Masoetsa, and I. Hussain, "A Narrative Review of the Benefits and Risks of Total Contact Casts in the Management of Diabetic Foot Ulcers," *J. Am. Coll. Clin. Wound Spec.*, vol. 9, no. 1–3, pp. 19–23, 2017.

[9] L. E. Gasca-lozano, S. Lucano-landeros, H. Ruiz-mercado, A. Salazar-montes, A. Sandoval-rodríguez, J. Garcia-bañuelos, A. Santos-garcia, J. R. Davila-rodriguez, J. Navarro-partida, H. Bojórquez-sepúlveda, J. Castañeda-gomez, J. Domínguez-rosales, M. A. Ruiz-arcos, M. G. Sánchez-parada, and J. Armendariz-borunda, "Clinical Study Pirfenidone Accelerates Wound Healing in Chronic Diabetic Foot Ulcers : A Randomized , Double-Blind Controlled Trial," vol. 2017, 2017.

[10] M. Hoffmann, P. Kujath, A. Flemming, M. Proß, N. Begum, M. Zimmermann, T. Keck, M. Kleemann, and E. Schloericke, "Survival of diabetes patients with major amputation is comparable to malignant disease," *Diabetes Vasc. Dis. Res.*, vol. 12, no. 4, pp. 265–271, 2015.

[11] "Activity Patterns of Patients With Diabetic Foot Ulceration," vol. 26, no. 9, 2003.

[12] C. Care, "Use of Pressure Offloading Devices in," vol. 31, no. 11, 2008.

[13] T. Y. Ryu, J. Park, and P. E. Scherer, "Hyperglycemia as a risk factor for cancer progression," *Diabetes and Metabolism Journal*. 2014.

[14] C. Library, "Treatment of the diabetic foot by offloading: a systematic review."

[15] M. Bartoli, X. Gu, N. T. Tsai, R. C. Venema, S. E. Brooks, M. B. Marrero, and R. B. Caldwell, "Vascular endothelial growth factor activates STAT proteins in aortic endothelial cells," *J. Biol. Chem.*, vol. 275, no. 43, pp. 33189–33192, 2000.

[16] R. T. Crews, B. Shen, L. Campbell, P. J. Lamont, A. J. M. Boulton, M. Peyrot, R. S. Kirsner, L. Vileikyte, C. Care, and E. Nutrition, "Role and Determinants of Adherence to Off-loading in Diabetic Foot Ulcer Healing : A Prospective Investigation," vol. 39, no. August, pp. 1371–1377, 2016.

[17] W. Lafayette, "A comparative analysis of skin substitutes used in the management of

diabetic foot ulcers," 2014.

[18] S. Tb, P. Ppc, and U. Dt, "Skin grafting and tissue replacement for treating foot ulcers in people with diabetes (Review)," no. 2, 2017.

[19] K. E. Johnson and T. A. Wilgus, "Vascular Endothelial Growth Factor and Angiogenesis in the Regulation of Cutaneous Wound Repair," vol. 3, no. 10, pp. 647–661, 2014.

[20] T. M. Honnegowda, P. Kumar, E. Govindarama, P. Udupa, S. Kumar, U. Kumar, and P. Rao, "Role of angiogenesis and angiogenic factors in acute and chronic wound healing," 2015.

[21] P. Bao, A. Kodra, M. Tomic-canic, D. Ph, M. S. Golinko, H. P. Ehrlich, D. Ph, and H. Brem, "The Role of Vascular Endothelial Growth Factor in Wound Healing," *YJSRE*, vol. 153, no. 2, pp. 347–358, 2009.

[22] Z. Chen, S. Fu, Z. Wu, J. Chen, Y. Huang, Y. Wang, and M. Fu, "Clinica Chimica Acta Relationship between plasma angiogenic growth factors and diabetic foot ulcers," *Clin. Chim. Acta*, vol. 482, no. January, pp. 95–100, 2018.

[23] B. Salvador, A. Arranz, S. Francisco, L. Córdoba, C. Punzón, M. Ángel, and M. Fresno, "Modulation of endothelial function by Toll like receptors," *Pharmacol. Res.*, vol. 108, pp. 46–56, 2016.

[24] S. Saberianpour, M. Heidarzadeh, M. H. Geranmayeh, and H. Hosseinkhani, "Tissue engineering strategies for the induction of angiogenesis using biomaterials," vol. 4, pp. 1–15, 2018.

[25] M. Lovett, D. Ph, K. Lee, D. Ph, A. Edwards, D. Ph, D. L. Kaplan, and D. Ph, "Vascularization Strategies for Tissue Engineering," vol. 15, no. 3, 2009.

[26] J. J. Kim, L. Hou, and N. F. Huang, "HHS Public Access," no. 650, pp. 17–26, 2017.

[27] H. G. Song, R. T. Rumma, C. K. Ozaki, E. R. Edelman, and C. S. Chen, “Review Vascular Tissue Engineering : Progress , Challenges , and Clinical Promise,” *Stem Cell*, vol. 22, no. 3, pp. 340–354, 2018.

[28] Z. Gu, J. Fu, H. Lin, and Y. He, “Development of 3D Bioprinting: From Printing Methods to Biomedical Applications,” *Asian J. Pharm. Sci.*, 2019.

[29] W. C. Wilson and T. Boland, “Cell and organ printing 1: Protein and cell printers,” *Anat. Rec. - Part A Discov. Mol. Cell. Evol. Biol.*, vol. 272, no. 2, pp. 491–496, 2003.

[30] T. Boland, V. Mironov, A. Gutowska, E. A. Roth, and R. R. Markwald, “Cell and organ printing 2: Fusion of cell aggregates in three-dimensional gels,” *Anat. Rec. - Part A Discov. Mol. Cell. Evol. Biol.*, vol. 272, no. 2, pp. 497–502, 2003.

[31] T. Boland, T. Xu, B. Damon, and X. Cui, “Application of inkjet printing to tissue engineering,” *Biotechnol. J.*, vol. 1, no. 9, pp. 910–917, 2006.

[32] G. D. Martin, S. D. Hoath, and I. M. Hutchings, “Inkjet printing - The physics of manipulating liquid jets and drops,” *J. Phys. Conf. Ser.*, vol. 105, no. 1, pp. 0–14, 2008.

[33] C. De Maria, J. Rincon, A. A. Duarte, G. Vozzi, and T. Boland, “A new approach to fabricate agarose microstructures,” *Polym. Adv. Technol.*, vol. 24, no. 10, pp. 895–902, 2013.

[34] X. Cui and T. Boland, “Human microvasculature fabrication using thermal inkjet printing technology,” *Biomaterials*, vol. 30, no. 31, pp. 6221–6227, 2009.

[35] M. Yanez, J. Rincon, A. Dones, C. De Maria, R. Gonzales, and T. Boland, “*In Vivo* Assessment of Printed Microvasculature in a Bilayer Skin Graft to Treat Full-Thickness Wounds,” *Tissue Eng. Part A*, vol. 21, no. 1–2, pp. 224–233, 2015.

[36] A. B. Fisher, A. B. Al-Mehdi, and Y. Manevich, “Shear stress and endothelial cell

activation," *Crit. Care Med.*, vol. 30, no. 5 SUPPL., 2002.

[37] R. Chang, J. Nam, and W. Sun, "Effects of Dispensing Pressure and Nozzle Diameter on Cell Survival from Solid Freeform Fabrication–Based Direct Cell Writing," *Tissue Eng. Part A*, vol. 14, no. 1, pp. 41–48, 2008.

[38] S. V. Murphy and A. Atala, "3D bioprinting of tissues and organs," *Nature Biotechnology*, vol. 32, no. 8. pp. 773–785, 2014.

[39] J. Li, M. Chen, X. Fan, and H. Zhou, "Recent advances in bioprinting techniques: Approaches, applications and future prospects," *J. Transl. Med.*, vol. 14, no. 1, 2016.

[40] Y. S. Zhang, K. Yue, J. Aleman, K. Mollazadeh-Moghaddam, S. M. Bakht, J. Yang, W. Jia, V. Dell'Erba, P. Assawes, S. R. Shin, M. R. Dokmeci, R. Oklu, and A. Khademhosseini, "3D Bioprinting for Tissue and Organ Fabrication," *Ann. Biomed. Eng.*, vol. 45, no. 1, pp. 148–163, 2017.

[41] B. R. Ringeisen, R. K. Pirlo, P. K. Wu, T. Boland, Y. Huang, W. Sun, Q. Hamid, and D. B. Chrisey, "Cell and organ printing turns 15: Diverse research to commercial transitions," *MRS Bull.*, 2013.

[42] S. Ji and M. Guvendiren, "Recent Advances in Bioink Design for 3D Bioprinting of Tissues and Organs," *Front. Bioeng. Biotechnol.*, vol. 5, 2017.

[43] K. J. L. Burg, D. Dréau, and T. Burg, *Engineering 3D Tissue Test Systems*. CRC Press, 2017.

[44] J. Rouwkema and A. Khademhosseini, "Vascularization and Angiogenesis in Tissue Engineering : Beyond Creating Static Networks," *Trends Biotechnol.*, vol. 34, no. 9, pp. 733–745, 2016.

[45] P. Dan, E. Velot, V. Decot, and P. Menu, "The role of mechanical stimuli in the vascular

differentiation of mesenchymal stem cells," *J. Cell Sci.*, 2015.

[46] C. J. Miller and L. A. Davidson, "The interplay between cell signalling and mechanics in developmental processes," *Nature Reviews Genetics*. 2013.

[47] Y. J. Lee, H. J. Lee, S. H. Choi, Y. B. Jin, H. J. An, J. H. Kang, S. S. Yoon, and Y. S. Lee, "Soluble HSPB1 regulates VEGF-mediated angiogenesis through their direct interaction," *Angiogenesis*, 2012.

[48] J. Sawada, F. Li, and M. Komatsu, "R-Ras Inhibits VEGF-Induced p38MAPK Activation and HSP27 Phosphorylation in Endothelial Cells," *J. Vasc. Res.*, 2016.

[49] A. Yuno, M. J. Lee, S. Lee, Y. Tomita, D. Rekhtman, B. Moore, and J. B. Trepel, "Clinical evaluation and biomarker profiling of Hsp90 inhibitors," in *Methods in Molecular Biology*, 2018.

[50] D. Schilling, C. Garrido, S. E. Combs, and G. Multhoff, "The Hsp70 inhibiting peptide aptamer A17 potentiates radiosensitization of tumor cells by Hsp90 inhibition," *Cancer Lett.*, 2017.

[51] C. De Maria, J. Rincon, A. A. Duarte, G. Vozzi, and T. Boland, "A new approach to fabricate agarose microstructures," *Polym. Adv. Technol.*, vol. 24, no. 10, pp. 895–902, 2013.

[52] and R. J. A. Denisse A. Gutierrez, Rebecca E. DeJesus, Lisett Contreras, Isela A. Rodriguez-Palomares, Paulina J. Villanueva, Karol S. Balderrama, Lenore Monterroza, Manuel Larragoity, Armando Varela-Ramirez, "A new pyridazinone exhibits potent cytotoxicity on human cancer cells via apoptosis and poly-ubiquitinated protein accumulation," *Cell Biol. Toxicol.*, vol. In Press, 2019.

[53] Q. R.-C. Blanca F. Iglesias-Figueroa, Tania S. Siqueiros-Cendon, Denisse A. Gutierrez,

Renato J. Aguilera, Edward A. Espinoza, Sigifredo Arevalo-Gallegos, Armando Varela-Ramirez, “Human recombinant lactoferrin induces apoptosis, disruption of F-actin structure and cell cycle arrest with selective cytotoxicity on human triple negative breast cancer cells.,” *Apoptosis*, vol. Under Revi, 2019.

[54] A. Varela-Ramirez, M. Costanzo, Y. P. Carrasco, K. H. Pannell, and R. J. Aguilera, “Cytotoxic effects of two organotin compounds and their mode of inflicting cell death on four mammalian cancer cells,” *Cell Biol. Toxicol.*, 2011.

[55] B. E. Ruiz-Medina, D. Lerma, M. Hwang, J. A. Ross, R. Skouta, R. J. Aguilera, R. A. Kirken, A. Varela-Ramirez, and E. Robles-Escajeda, “Green barley mitigates cytotoxicity in human lymphocytes undergoing aggressive oxidative stress, via activation of both the Lyn/PI3K/Akt and MAPK/ERK pathways,” *Sci. Rep.*, 2019.

[56] E. Robles-escajeda, D. Lerma, A. M. Nyakeriga, J. A. Ross, R. A. Kirken, R. J. Aguilera, and A. Varela-ramirez, “Searching in Mother Nature for Anti-Cancer Activity : Anti-Proliferative and Pro-Apoptotic Effect Elicited by Green Barley on Leukemia / Lymphoma Cells,” vol. 8, no. 9, pp. 1–18, 2013.

[57] X. Cui, D. Dean, Z. M. Ruggeri, and T. Boland, “Cell damage evaluation of thermal inkjet printed chinese hamster ovary cells,” *Biotechnol. Bioeng.*, vol. 106, no. 6, pp. 963–969, 2010.

[58] K. Segawa and S. Nagata, “An Apoptotic ‘Eat Me’ Signal: Phosphatidylserine Exposure,” *Trends in Cell Biology*. 2015.

[59] E. Robles-escajeda, U. Das, N. M. Ortega, K. Parra, G. Francia, J. R. Dimmock, A. Varela-ramirez, and R. J. Aguilera, “HHS Public Access,” vol. 39, no. 3, pp. 265–277, 2016.

[60] P. J. Villanueva, A. Martinez, S. T. Baca, R. E. Dejesus, M. Larragoity, L. Contreras, D. A. Gutierrez, A. Varela-ramirez, and R. J. A. Id, “Pyronaridine exerts potent cytotoxicity on human breast and hematological cancer cells through induction of apoptosis,” pp. 1–18, 2018.

[61] L. Contreras, R. I. Calderon, A. Varela-ramirez, H. Zhang, and Y. Quan, “Induction of apoptosis via proteasome inhibition in leukemia / lymphoma cells by two potent piperidones,” pp. 623–636, 2018.

[62] J. Xiang, C. Wan, R. Guo, and D. Guo, “Is Hydrogen Peroxide a Suitable Apoptosis Inducer for All Cell Types?,” *Biomed Res. Int.*, vol. 2016, 2016.

[63] C. Brana, C. Benham, and L. Sundstrom, “A method for characterising cell death in vitro by combining propidium iodide staining with immunohistochemistry,” *Brain Res. Protoc.*, 2002.

[64] Y. Nicolau, F. Bany-Mohammed, C. L. Cai, J. V. Aranda, and K. D. Beharry, “SiRNA silencing of VEGF, IGFs, and their receptors in human retinal microvascular endothelial cells,” *Am. J. Transl. Res.*, 2018.

[65] O. Kaplan, J. Zárubová, B. Mikulová, E. Filová, J. Bártová, L. Baèáková, and E. Brynda, “Enhanced mitogenic activity of recombinant human vascular endothelial growth factor VEGF121 expressed in E. coli Origami B (DE3) with molecular chaperones,” *PLoS One*, 2016.

[66] A. Weber, P. Wasiliew, and M. Kracht, “Interleukin-1 (IL-1) Pathway,” vol. 3, no. 105, pp. 1–7, 2010.

[67] B. Henderson and F. Kaiser, “Do reciprocal interactions between cell stress proteins and cytokines create a new intra-/extra-cellular signalling nexus?,” *Cell Stress Chaperones*,

2013.

[68] N. G. dela Paz, T. E. Walshe, L. L. Leach, M. Saint-Geniez, and P. A. D'Amore, "Role of shear-stress-induced VEGF expression in endothelial cell survival," *J. Cell Sci.*, 2012.

[69] A. Kishor, B. Tandukar, Y. V Ly, E. A. Toth, Y. Suarez, G. Brewer, and G. M. Wilson, "Hsp70 Is a Novel Posttranscriptional Regulator of Gene Expression That Binds and Stabilizes Selected mRNAs Containing AU-Rich," vol. 33, no. 1, pp. 71–84, 2013.

[70] D. J. J. Waugh and C. Wilson, "The interleukin-8 pathway in cancer," *Clinical Cancer Research*. 2008.

[71] Y. Ning, P. C. Manegold, Y. K. Hong, W. Zhang, A. Pohl, G. Lurje, T. Winder, D. Yang, M. J. LaBonte, P. M. Wilson, R. D. Ladner, and H. J. Lenz, "Interleukin-8 is associated with proliferation, migration, angiogenesis and chemosensitivity in vitro and in vivo in colon cancer cell line models," *Int. J. Cancer*, vol. 128, no. 9, pp. 2038–2049, 2011.

[72] D. Martin, R. Galisteo, and J. S. Gutkind, "CXCL8/IL8 stimulates vascular endothelial growth factor (VEGF) expression and the autocrine activation of VEGFR2 in endothelial cells by activating NFκB through the CBM (Carma3/Bcl10/Malt1) complex," *J. Biol. Chem.*, 2009.

[73] W. S. Moon, D. Ph, K. H. Rhyu, M. Sc, M. J. Kang, D. Ph, D. G. Lee, D. Ph, H. C. Yu, D. Ph, J. H. Yeum, G. Y. Koh, D. Ph, A. S. Tarnawski, and D. Sc, "Overexpression of VEGF and Angiopoietin 2 : A Key to High Vascularity of Hepatocellular Carcinoma ?," vol. 1, pp. 1–6.

[74] M. Kitade, M. Uemura, T. Masaki, and H. Fukui, "Angiopoietin 2 displays a vascular endothelial growth factor dependent synergistic effect in hepatocellular carcinoma development in mice," vol. 1, pp. 1768–1775, 2005.

[75] E. Fagiani and G. Christofori, “Angiopoietins in angiogenesis,” *Cancer Letters*. 2013.

[76] R. M. Pedrigi, K. I. Papadimitriou, A. Kondiboyina, S. Sidhu, J. Chau, M. B. Patel, D. C. Baeriswyl, E. M. Drakakis, and R. Krams, “Disturbed Cyclical Stretch of Endothelial Cells Promotes Nuclear Expression of the Pro-Atherogenic Transcription Factor NF-κB,” *Ann. Biomed. Eng.*, vol. 45, no. 4, pp. 898–909, 2017.

[77] N. F. Jufri, A. Mohamedali, A. Avolio, and M. S. Baker, “Mechanical stretch: Physiological and pathological implications for human vascular endothelial cells,” *Vasc. Cell*, vol. 7, no. 1, pp. 1–12, 2015.

[78] M. Blazincic, “Physics of Ink-jet Printing,” *Dept. Appl. Math., Univ. Birmingham Kodak Eur. Res.*, no. June 2008, pp. 1–10, 2008.

[79] T. Boland, “Personal Communication.” 2020.

[80] T. K. Kim, H. J. Na, W. R. Lee, M. H. Jeoung, and S. Lee, “Heat shock protein 70-1A is a novel angiogenic regulator,” *Biochem. Biophys. Res. Commun.*, 2016.

[81] S. L. Park, T. W. Chung, S. Kim, B. Hwang, J. M. Kim, H. M. Lee, H. J. Cha, Y. Seo, S. Y. Choe, K. T. Ha, G. Kim, S. J. Yun, S. S. Park, Y. H. Choi, B. K. Kim, W. T. Kim, E. J. Cha, C. Patterson, W. J. Kim, *et al.*, “HSP70-1 is required for interleukin-5-induced angiogenic responses through eNOS pathway,” *Sci. Rep.*, 2017.

[82] C. Lieu, J. Heymach, M. Overman, H. Tran, and S. Kopetz, “Beyond VEGF: Inhibition of the fibroblast growth factor pathway and antiangiogenesis,” *Clinical Cancer Research*. 2011.

[83] Z. K. Otrock, R. A. R. Mahfouz, J. A. Makarem, and A. I. Shamseddine, “Understanding the biology of angiogenesis: Review of the most important molecular mechanisms,” *Blood Cells, Molecules, and Diseases*. 2007.

[84] L. H. W. Gowdak and J. E. Krieger, “Vascular Growth Factors, Progenitor Cells, and Angiogenesis,” *Endothel. Cardiovasc. Dis. Vasc. Biol. Clin. Syndr.*, pp. 49–62, 2018.

[85] D. Gomez and N. C. Reich, “Stimulation of Primary Human Endothelial Cell Proliferation by IFN,” *J. Immunol.*, vol. 170, no. 11, pp. 5373–5381, 2003.

[86] X. Q. Werdich and J. S. Penn, “Src, Fyn and Yes play differential roles in VEGF-mediated endothelial cell events,” *Angiogenesis*, vol. 8, no. 4, pp. 315–326, 2006.

[87] “homeAction @ www.phosphosite.org.” .

[88] P. R. Somanath, O. V. Razorenova, J. Chen, and T. V. Byzova, “Akt1 in endothelial cell and angiogenesis,” *Cell Cycle*, vol. 5, no. 5, pp. 512–518, 2006.

[89] M. A. Farhan, K. Carmine-Simmen, J. D. Lewis, R. B. Moore, and A. G. Murray, “Endothelial cell mTOR complex-2 regulates sprouting angiogenesis,” *PLoS One*, vol. 10, no. 8, pp. 1–20, 2015.

[90] J. A. McCubrey, L. S. Steelman, F. E. Bertrand, N. M. Davis, M. Sokolosky, S. L. Abrams, G. Montalto, A. B. D’Assoro, M. Libra, F. Nicoletti, R. Maestro, J. Basecke, D. Rakus, A. Gizak, Z. Demidenko, L. Cocco, A. M. Martelli, and M. Cervello, “GSK-3 as potential target for therapeutic intervention in cancer,” *Oncotarget*, vol. 5, no. 10, 2014.

[91] J. Ma, L. Zhang, W. Han, T. Shen, C. Ma, Y. Liu, X. Nie, M. Liu, Y. Ran, and D. Zhu, “Activation of JNK/c-Jun is required for the proliferation, survival, and angiogenesis induced by EET in pulmonary artery endothelial cells,” *J. Lipid Res.*, vol. 53, no. 6, pp. 1093–1105, 2012.

[92] J. X. Zhao, W. F. Yue, M. J. Zhu, and M. Du, “AMP-activated protein kinase regulates β-catenin transcription via histone deacetylase 5,” *J. Biol. Chem.*, vol. 286, no. 18, pp. 16426–16434, 2011.

[93] J. Ahn, M. Urist, and C. Prives, “The Chk2 protein kinase,” *DNA Repair (Amst).*, vol. 3, no. 8–9, pp. 1039–1047, 2004.

[94] C. Koteswara Rao, T. Mohammad, S. Tiffany, and M. Dolly, “Cyclic AMP response element-binding protein prevents endothelial permeability increase through transcriptional controlling p190RhoGAP expression.,” *Blood*, vol. 119, no. 1, pp. 308–319, 2011.

[95] C. Uchida, E. Gee, E. Ispanovic, and T. L. Haas, “JNK as a positive regulator of angiogenic potential in endothelial cells,” vol. 32, pp. 769–776, 2008.

[96] S. Chien, “Mechanotransduction and endothelial cell homeostasis: The wisdom of the cell,” *Am. J. Physiol. - Hear. Circ. Physiol.*, vol. 292, no. 3, 2007.

[97] J. Wu, T. Liu, Z. Rios, Q. Mei, X. Lin, and S. Cao, “Heat Shock Proteins and Cancer,” *Trends in Pharmacological Sciences*. 2017.

[98] S. Chaudhuri and P. G. Smith, “Cyclic strain-induced HSP27 phosphorylation modulates actin filaments in airway smooth muscle cells,” *Am. J. Respir. Cell Mol. Biol.*, vol. 39, no. 3, pp. 270–278, 2008.

[99] A. Q. Sheikh, C. Kuesel, T. Taghian, J. R. Hurley, W. Huang, Y. Wang, R. B. Hinton, and D. A. Narmoneva, “Angiogenic microenvironment augments impaired endothelial responses under diabetic conditions,” *Am. J. Physiol. - Cell Physiol.*, vol. 306, no. 8, pp. 768–778, 2014.

[100] Z. Batulan, V. K. Pulakazhi Venu, Y. Li, G. Koumbadinga, D. G. Alvarez-Olmedo, C. Shi, and E. R. O’Brien, “Extracellular release and signaling by heat shock protein 27: Role in modifying vascular inflammation,” *Frontiers in Immunology*. 2016.

[101] D. Thuringer, G. Jego, G. Wettstein, O. Terrier, L. Cronier, N. Yousfi, S. Hébrard, A. Bouchot, A. Hazoumé, A. L. Joly, M. Gleave, M. Rosa-Calatrava, E. Solary, and C.

Garrido, “Extracellular HSP27 mediates angiogenesis through Toll-like receptor 3,” *FASEB J.*, 2013.

[102] C. S. Lin, P. J. He, W. T. Hsu, M. S. Wu, C. J. Wu, H. W. Shen, C. H. Hwang, Y. K. Lai, N. M. Tsai, and K. W. Liao, “Helicobacter pylori-derived heat shock protein 60 enhances angiogenesis via a CXCR2-mediated signaling pathway,” *Biochem. Biophys. Res. Commun.*, 2010.

[103] G. Pfister, C. M. Stroh, H. Perschinka, M. Kind, M. Knoflach, P. Hinterdorfer, and G. Wick, “Detection of HSP60 on the membrane surface of stressed human endothelial cells by atomic force and confocal microscopy,” *J.Cell Sci.*, 2005.

[104] N. R. Schiele, D. T. Corr, Y. Huang, N. A. Raof, Y. Xie, and D. B. Chrisey, “Laser-based direct-write techniques for cell printing,” *Biofabrication*. 2010.

[105] A. Townsend-Nicholson and S. N. Jayasinghe, “Cell electrospinning: A unique biotechnique for encapsulating living organisms for generating active biological microthreads/scaffolds,” *Biomacromolecules*, vol. 7, no. 12, pp. 3364–3369, 2006.

[106] M. F. Canbolat, C. Tang, S. H. Bernacki, B. Pourdeyhimi, and S. Khan, “Mammalian Cell Viability in Electrospun Composite Nanofiber Structures,” pp. 1346–1356.

[107] M. D. Sarker, S. Naghieh, N. K. Sharma, and X. Chen, “3D biofabrication of vascular networks for tissue regeneration: A report on recent advances,” *Journal of Pharmaceutical Analysis*, 2018.

Glossary

AKT	Protein Kinase B
AMPK	AMP-activated protein kinase
Ang	Angiopoietin
Chk2	Cell Cycle Checkpoint Kinase 2
CREB	Cyclic amp Response Element-Binding Protein
DFU	Diabetic Foot Ulcer
DM	Diabetes Mellitus
EC	Endothelial Cell
EGFR	Epidermal Growth Factor Receptor
eNOS	Endothelial Nitric-Oxide Synthase
ERK	Extracellular Signal-Regulated Kinase
FAK	Focal Adhesion Kinase
FGF	Fibroblast Growth Factor
FGFR	Fibroblast Growth Factor Receptor
GPCR	G-Protein Coupled Receptor
GSK	Glycogen Synthase Kinase
HMVEC	Human Microvascular Endothelial Cell
HS	Heat Shocked
HSP	Heat Shock Protein
IL	Interleukin
JNK	c-Jun N-terminal Kinase
MAPK	Mitogen-activated Protein Kinase
MP	Manually Pipetted
mTOR	Mammalian Target of Rapamycin
NF-κB	Nuclear Factor binding near the κ light-chain gene in B cells

PDGF	Platelet Derived Growth Factor
PI3K	Phosphoinositide 3-Kinase
PLC	Phospholipase C
PRAS40	Proline-rich AKT substrate
Pyk	Proline-rich Tyrosine Kinase
RCW	Removable Cast Walker
RSK	Ribosomal S6 Kinase
RTK	Receptor Tyrosine Kinase
Src	Sarcoma Tyrosine Kinase
STAT	Signal Transducers and Activator of Transcription
TCC	Total Contact Cast
TE	Tissue Engineering
TIB	Thermal Inkjet Bioprinter
TLR	Toll-like Receptor
VEGF	Vascular Endothelial Growth Factor
VEGFR	Vascular Endothelial Growth Factor Receptor
WNK	Lysine Deficient Protein Kinase

Vita

Luis H. Solis earned his B.S. in Microbiology from New Mexico State University (NMSU), where he then continued his graduate studies pursuing a Master's in Public Health. Years later he joined the Biomedical Device, Delivery, and Diagnostic (B3D) Laboratory at The University of Texas at El Paso (UTEP) under the supervision of Dr. Thomas Boland.

Luis' projects were focused in the arena of tissue engineering. At first, he was eager to gain valuable knowledge in the development of a thermal inkjet bioprinted (TIB) 3D bioartificial pancreas. Soon after, he realized that his beta-cell laden constructs were becoming necrotic within two weeks of culturing them. He attempted to co-culture beta- and endothelial-cells *in vitro,* but was not successful. It wasn't until he implanted these co-cultured cells that he found that TIB-ECs developed vast microvascular beds. It was at this point in time that his research interests changed to cellular and molecular biology and the signaling pathways that mediate cell survival in order to understand why TIB cells were becoming angiogenic.

While pursuing his Ph.D., Luis worked as a Teaching Assistant for the Departments of Biological and Rehabilitation Sciences at UTEP. A year later, he was awarded the Research Initiative for Scientific Enhancement (RISE) Fellowship Award from the Department of Biological Sciences. This prestigious award covers the student's tuition, stipend, and materials for four years allowing students to focus on their research. Luis was also awarded two Dodson Research Grants valued at approximately $6,000.00 combined. Finally, in his last year, he was awarded the Completion Dissertation Fellowship Award from the UTEP Graduate School.

Contact Information: lhorasolis@gmail.com